

Intra- and Intercrystalline Oxygen Isotope Variations in Minerals from Basalts and Peridotites

JOHN EILER^{1*}, EDWARD M. STOLPER¹ AND MOLLY C. McCANTA²

¹DIVISION OF GEOLOGICAL AND PLANETARY SCIENCES, CALIFORNIA INSTITUTE OF TECHNOLOGY, PASADENA, CA 91125, USA

²DEPARTMENT OF GEOLOGY, TUFTS UNIVERSITY, MEDFORD, MA 02155, USA

RECEIVED OCTOBER 3, 2010; ACCEPTED FEBRUARY 1, 2011
ADVANCE ACCESS PUBLICATION MAY 6, 2011

Igneous phenocrysts commonly exhibit zoning in major and trace element composition, reflecting (and potentially constraining) the differentiation and/or mixing histories of their parent melts. To date, little work has been done characterizing zonation of oxygen isotopes in minerals from mafic and ultramafic rocks. We present 259 ion probe (CAMECA ims-1280) measurements of $\delta^{18}\text{O}$ in 34 natural magmatic and mantle olivines and pyroxenes from five hand samples from diverse igneous environments. We compare $\delta^{18}\text{O}$ variations with zonation in other elements [especially P; analyzed by electron microprobe analysis (EMPA) and nano-secondary ionization mass spectrometry (nanoSIMS)]. There is generally a close (average within $\sim 0.1\text{--}0.2\text{‰}$) agreement between average $\delta^{18}\text{O}$ values of olivines measured by SIMS (standardized against San Carlos olivine) and independently known values for bulk separates from the same samples measured by laser fluorination. These data demonstrate that current ion microprobe techniques are not only precise but also accurate enough for study of sub-per-mil oxygen isotope variations in silicates (within $\sim 0.2\text{‰}$), provided samples are prepared and analyzed following strict guidelines. All but one of the 34 studied grains are homogeneous in $\delta^{18}\text{O}$ within a small multiple of analytical precision [estimated $\pm 0.2\text{‰}$, 1σ for most data; poorer for a subset of measurements made on small ($\sim 5\ \mu\text{m}$) spots]. This population of isotopically homogeneous grains includes some with oscillatory micrometer-scale P banding. The lack of $\delta^{18}\text{O}$ variations suggests that whatever factors lead to this common mode of trace element zonation have no detectable effect on melt–crystal partitioning of oxygen isotopes. Large (2‰) oxygen isotope variations are observed in one olivine glomerocryst from Mauna Kea, Hawaii. This glomerocryst contains P-rich domains that are either equant or skeletal or feathery in outline, and these P-rich domains are

systematically low in $\delta^{18}\text{O}$ compared with adjacent, later-grown, P-poor olivine. This unusual oxygen isotope zonation pattern might reflect a kinetic fractionation during nucleation and growth of the cores of some olivine phenocrysts. We tested this hypothesis through measurements of $\delta^{18}\text{O}$ distributions in synthetic olivines grown at a range of rates and exhibiting diverse patterns of P zoning. These synthetic olivines are homogeneous in $\delta^{18}\text{O}$, within the limits of our analyses ($\pm 0.3\text{--}0.4\text{‰}$ in this case) and show no connection between P zonation and oxygen isotope heterogeneity. We therefore think it more plausible that unusual O isotope zonation in the Mauna Kea glomerocryst reflects addition of a low- $\delta^{18}\text{O}$ component to some Hawaiian magmas just before nucleation of olivine. More generally, this study demonstrates the utility of modern SIMS techniques for in situ study of the subtle ($\sim 1\text{‰}$ range) oxygen isotope variations characteristic of common mafic and ultramafic rocks.

KEY WORDS: stable isotope; igneous; in situ

INTRODUCTION

Intracrystalline variations in the chemical and isotopic compositions of igneous minerals provide information regarding the origin and evolution of magmas. Such data can document variations in magma composition over the course of crystallization–differentiation and/or mixing processes (e.g. Kuritani, 1998; see review by Davidson *et al.*, 2007), and they can often help to constrain the compositions of primary melts (e.g. Yögodzinski & Kelemen, 1998). In some instances, such as detrital zircons or

*Corresponding author. E-mail: eiler@gps.caltech.edu

chromites, such information is the only way to reconstruct magma compositions, because the original hosts of these grains have been destroyed by weathering and/or metamorphism (Hanchar & Miller, 1993).

Previous studies have examined intracrystalline variations in major, minor, and trace element abundance in igneous materials based on three widely available micro-analytical techniques—the electron and ion microprobes and, more recently, laser-ablation inductively coupled plasma mass spectrometry (LA-ICMPS) (Jeffries *et al.*, 1995). Such data are the basis for studies of oscillatory and other elemental zonation patterns in igneous minerals (Hattori & Sato, 1996), phenocryst residence times (Hawkesworth *et al.*, 2000), magma mixing (Griffin *et al.*, 2002), and many other petrological phenomena (e.g., Griffin *et al.*, 1996). Observations of intracrystalline variations in the isotopic compositions of igneous materials are, however, more sparse. Ion microprobe measurements of Pb isotopes in zircons and other U- and Th-rich accessory minerals are commonly made as a component of geochronological studies (Zhou *et al.*, 2002), and there is a smaller but growing body of LA-ICMPS measurements of Sr isotopes in feldspars (Davidson *et al.*, 1990) and of Pb and Hf isotopes in zircons (Griffin *et al.*, 2002). However, *in situ* oxygen isotope analysis of zircons is perhaps the only example of a stable isotope measurement that has produced abundant data documenting intracrystalline variations in an igneous material (Bindeman *et al.*, 2008a); Bindeman *et al.* (2008b) and Wang & Eiler (2008) presented such data for Icelandic and Hawaiian olivines, respectively. This relative paucity of data on intracrystalline isotopic variations reflects the difficulty of precisely measuring isotopic ratios of microgram and smaller quantities of minerals. Previous attempts to ‘harvest’ milligram quantities of texturally distinct mineral separates have permitted isotopic analyses that constrain intracrystalline zonation (e.g. Baker *et al.*, 2000), but this approach is applicable only to rocks in which minerals are distinctively and consistently zoned in color, density, or some other physical property, and, more generally, it provides only a loose connection to grain-scale textural features. Laser-based techniques for *in situ* light stable isotope analysis are available (Rumble *et al.*, 1997; Wang & Eiler, 2008), but they are generally difficult and have spatial domains too large ($\geq 100 \mu\text{m}$) for many problems. The most recent generation of multi-collector, large-radius ion microprobes provides the only practical means of pursuing such work in a broad and systematic fashion (e.g. Kita *et al.*, 2009; Valley & Kita, 2009). A remaining problem with these techniques is that matrix effects prevent standardization of compositionally complex phases with an accuracy equal to the current precision of a single analytical spot (e.g. Eiler *et al.*, 1997; Page *et al.*, 2010). However, this problem appears to be minimal when studying

stoichiometric phases having limited ranges of cation chemistry (e.g. Mg-rich olivines; Valley & Kita, 2009; Kita *et al.*, 2009).

Here, we describe the oxygen isotope distributions in olivines and pyroxenes from natural basalts and mantle peridotites and in olivines grown experimentally from synthetic melts. One motivation for this work is to provide a survey of the character of oxygen isotope variations in diverse mafic and ultramafic igneous materials at scales smaller than single mineral grains. Such variations have the potential to illuminate the causes of oxygen isotope variations at larger scales (i.e. between lavas) and/or to provide new constraints on processes of magmatic differentiation; thus it is useful to gain a general appreciation of the frequency, amplitudes, and patterns of oxygen isotope zonation. We also explore the suggestion from several recent studies that stable isotope ratios of igneous materials may be influenced by non-equilibrium partitioning between solids and melts. For example, it has been shown that Fe isotope variations between olivine separates (Teng *et al.*, 2008) and Li isotope gradients within single olivine phenocrysts (Gallagher & Elliott, 2009; Jeffcoate *et al.*, 2007) are consistent with the influence of sub-solidus, diffusive fractionations. Additionally, experimental studies of chemical diffusion in melts show that such processes can generate multiple-per-mil gradients in stable isotope ratios (Richter *et al.*, 2003). These studies raise the possibility that oxygen isotope distributions in igneous minerals might also be controlled by diffusive fractionations. Finally, a variety of igneous minerals commonly exhibit zonation in minor and trace element concentrations that can be understood as consequences of non-equilibrium melt–solid partitioning during phenocryst growth. Examples include oscillatory zonation of P in olivine (Milman-Barris *et al.*, 2008) and various trace elements responsible for cathodoluminescence zonation in zircon (Hanchar & Miller, 1993; Hofmann *et al.*, 2009). It has been suggested that such phenomena reflect diffusion-limited growth at melt–solid interfaces (Watson & Muller, 2009) and/or non-equilibrium partitioning on the surfaces of growing crystals (Watson, 1996). It is conceivable that such processes could result in non-equilibrium isotope fractionations (Jambon, 1980). Any zonation produced in these environments is likely to persist; volume diffusion of oxygen in olivine at magmatic temperatures is relatively slow (e.g. relaxation of gradients over a characteristic diffusion length scale of $100 \mu\text{m}$ requires $\sim 10^4$ years, assuming 1200°C and dry diffusion; Reddy *et al.*, 1980).

The methods of sample preparation and analysis are detailed in the Electronic Appendix (available at <http://petrology.oxfordjournals.org/>). Briefly, all analyzed samples are hand-picked grains that were mounted in epoxy and then polished. Major and minor element analyses were obtained by electron microprobe. Oxygen isotope analyses

were made with either a CAMECA ims-1280 large-radius, multi-collector ion microprobe or a CAMECA ims-7f geo, a smaller radius, single-collector ion microprobe.

We also present semi-quantitative maps of P distribution within a subset of the grains we have studied (generated by X-ray mapping on the electron microprobe), and for one grain we report quantitative *in situ* analyses of P concentration made with the CAMECA NanoSIMS 50L high-spatial-resolution ion microprobe in the same locations as the O isotope measurements (i.e. so we can confidently compare variations in $\delta^{18}\text{O}$ with variations in P). The instrumentation and methods of these analyses are also presented in the Electronic Appendix.

The oxygen isotope geochemistry of basaltic and mantle rocks

The oxygen isotope data we present can be interpreted in the context of the large number of previous studies of the oxygen isotope variations of igneous materials (Eiler, 2001, and references therein). Briefly, sedimentary, weathered, and/or aqueously altered crustal materials commonly exhibit large (multiple per mil to tens of per mil) enrichments or depletions in $^{18}\text{O}/^{16}\text{O}$ relative to the bulk mantle, which has a $\delta^{18}\text{O}_{\text{SMOW}}$ value of $\sim 5.5 \pm 0.2$ ‰ (Matthey *et al.*, 1994). These variations result from relatively low-temperature ($\leq \sim 300^\circ\text{C}$) exchange of oxygen between rocks and coexisting fluids. Therefore, the oxygen isotope ratios of igneous minerals and glasses potentially constrain the roles of crustal materials in magma genesis, either as subducted or lithospheric source components or as lithospheric contaminants added during differentiation. Because oxygen isotopes are subtly but measurably ($\leq \sim 1$ ‰) fractionated among minerals, melts, and vapor at magmatic temperatures, oxygen isotope measurements also can be used to study processes of partial melting, crystallization–differentiation, and magma degassing. Most studies of the oxygen isotope ratios of igneous rocks must make some effort to discriminate between isotopic variations among source components vs fractionations during melting and differentiation. This distinction is particularly important (and difficult) for studies of mafic igneous rocks, which typically vary only subtly in $\delta^{18}\text{O}$ (≤ 1 ‰).

Most of the existing data on the stable isotope ratios of igneous and mantle rocks come from bulk measurements of mineral separates, glasses, and whole-rocks, generally in milligram and larger quantities. Such data generally average intracrystalline and intercrystalline variability, with two potential disadvantages: it is often unclear to what degree measured variations among milligram-sized samples reflect partially homogenized intracrystalline variations as opposed to larger-scale variations (such as between hand samples); as a result, information that might be recorded by intracrystalline variations (e.g. isotopic changes of magmas over the course of differentiation) is often obscured. However, there are exceptions to this

among available data. For example, as noted above, some previous studies have constrained intracrystalline zonation by recovering milligram-quantities of mineral separates that concentrate grain rims vs cores based on color or other properties (e.g. Baker *et al.*, 2000). There is also a relatively large and diverse body of data describing oxygen isotope variations in single zircons based on *in situ* analyses using the ion microprobe (e.g. Bindeman *et al.*, 2008a; Valley, 2010; Grimes *et al.*, 2011). Finally, there are a smaller number of prior studies of *in situ* variations of O isotopes in olivines from basaltic lavas using *in situ* laser fluorination techniques (e.g. Wang & Eiler, 2008) or the ion microprobe (Bindeman *et al.*, 2008b).

SAMPLES AND METHODS

We present *in situ* oxygen isotope analyses for 34 grains of olivine and pyroxene from basalts and mantle peridotites and for several olivines grown in the laboratory from synthetic basaltic melts. Natural olivines and pyroxenes analyzed in this study come from the following samples: (1) three basalts—one relatively high in $\delta^{18}\text{O}$ (S500-5b, from Koolau volcano, Hawaii; Wang, 2005), and two relatively low in $\delta^{18}\text{O}$ [R215-7.2, from Mauna Kea volcano, Hawaii (Wang *et al.*, 2003) and 98MI from Theistareykir volcano, Iceland (Eiler *et al.*, 2001)]; (2) a metasomatized lherzolite from a subduction zone environment [nodule B3N from Batan, Philippines; Maury *et al.*, 1992; note our data for this sample are reproduced from Eiler *et al.* (2007), but used the same methods and standards as the other data reported here; (3) and an unmetasomatized lherzolite from the continental lithospheric mantle (San Carlos, New Mexico). This is a common and widely studied material; the oxygen isotope ratio of the aliquot from which the crystals analyzed here were taken was analyzed using laser fluorination by Eiler *et al.* (1995). Synthetic olivines were analyzed from two experiments (MPDA-26 and MPDA-32, from McCanta *et al.*, 2009), in which a basaltic liquid was cooled at a controlled rate.

Detailed descriptions and citations to previously published work on the samples studied here are as follows.

R215-7.2, Mauna Kea basalt

This shield-building tholeiite was recovered by the Hawaiian Scientific Drilling Project and has been previously studied for its whole-rock geochemistry and the oxygen isotope ratios of bulk olivine separates. Previous oxygen isotope measurements of this sample and associated references describing its geological setting and its geochemistry have been given by Eiler *et al.* (1996).

S500-5b Koolau basalt

This sample of shield-building tholeiite was recovered from a submarine landslide block by submersible. It has

been previously studied for its whole-rock major, trace element, and radiogenic isotope geochemistry and the oxygen isotope geochemistry of bulk olivine separates. Previous oxygen isotope and other geochemical data and a description of the sample location have been given by Wang *et al.* (2003) and in the references therein.

98M1 Iceland basalt

This lava was collected from an outcrop of recent olivine-phyric basalt on Theistareykir volcano, Iceland. This rift-zone tholeiite has been previously studied for its whole-rock major, trace element, and radiogenic isotope geochemistry and for the oxygen isotope geochemistry of bulk olivine separates. The geological setting and supporting geochemical data for this sample have been given by Eiler *et al.* (2001) and in the references therein.

B3N Batan xenolith

This mantle xenolith was collected from a high-K basaltic andesite erupted ≤ 1.48 kyr ago from Mount Iraya, Batan Island (Maury *et al.*, 1992; Schiano *et al.*, 1995; Eiler *et al.*, 2007). B3N is a deformed and metasomatized spinel harzburgite that contains neoblasts of Fe-rich olivine (Fo_{78–90}) and orthopyroxene (En_{86–88}) and various hydrous metasomatic minerals. (Richard *et al.*, 1986; Maury *et al.*, 1992; Schiano *et al.*, 1995). Our analyses focused on olivine neoblasts. Oxygen isotope ratios of melt inclusions from this sample have been presented by Eiler *et al.* (2007).

San Carlos xenolith

This spinel harzburgite nodule collected from San Carlos, Arizona is from the mineralogical collection of Caltech's Division of Geological and Planetary Sciences. Separates of San Carlos olivine are routinely used as an oxygen isotope secondary standard in laser fluorination laboratories (e.g. Eiler *et al.*, 1995, 2001, 2005, 2007; Wang *et al.*, 2003).

Experimental charges

We analyzed olivine from two synthetic aggregates of olivine and synthetic basaltic melt grown in dynamic crystallization experiments run in a vertical 1 atm gas-mixing furnace at Caltech using the wire-loop technique. The starting composition was a natural Hawaiian basalt (BHVO-2) doped with 10% olivine (Fo₉₂). Runs were taken to 1280°C (just above the liquidus), held for 3 h to homogenize, cooled at a constant rate to 1150°C to induce crystallization, and then drop quenched into deionized water. The experiments and run products will be described in more detail in a subsequent publication.

Sample preparation and analysis

Natural samples were coarsely crushed in a stainless steel percussion mortar, and millimeter-sized grain fragments of olivine and/or pyroxene were selected by hand picking under a binocular microscope. Selected grains were

cleaned in acetone, rinsed in ethanol, and dried in a 100°C oven. Cleaned grains were then mounted in high-vacuum epoxy, polished with emery paper down to 3 µm grit, then polished with alumina powder down to 0.1 µm grit, and finally gold coated prior to ion microprobe analysis.

Synthetic samples were cut, mounted in epoxy, and polished with diamond paper down to 5 µm grit and with diamond paste to 0.5 µm grit. Samples were then C-coated for electron microprobe analysis. This carbon coat was removed and replaced with an Au coat prior to ion microprobe analysis.

Most sample grains were prepared in epoxy adjacent to grains of a San Carlos olivine intralaboratory standard and then polished to a flat, smooth surface using alumina powder. Kita *et al.* (2009) have presented specific guidelines for grain flatness (≤ 3 µm topography) and spacing (within 5 mm of the center of a 2.5 cm diameter mount), which were followed for most samples. Most mounts included one or more grains that were ~ 1 –2 mm outside this ideal limit of 5 mm from the mount center. On the basis of data presented by Kita *et al.* (2009), it is possible that grain position contributed ~ 0.1 –0.2‰ to analytical errors for these grains; however, we noted no systematic differences between them and other grains with regard to intragrain reproducibility or average value, and published data are unclear as to how grain position relates to such analytical artefacts; therefore we have not culled any data on this basis. A subset of samples (indicated in all relevant tables and figures) were mounted separately in epoxy in 5 mm diameter brass 'bullets' that were then fitted into a single six-hole, 1 inch diameter brass disk. This is a common method for mounting samples for ion and electron microprobe analysis, but has potential to result in greater sample topography than the method recommended by Kita *et al.* (2009). We present here scanning electron microscope (SEM) and X-ray map images of only the subset of samples that exhibit significant texturally correlated isotopic variations; SEM and optical images of all analyzed grains are available on request from the corresponding author.

Most of the oxygen isotope data presented in this study were generated on the CAMECA ims-1280 ion microprobe at the University of Wisconsin using techniques that have been previously described (Eiler *et al.*, 2007; Kita *et al.*, 2009; Valley & Kita, 2009). These methods are detailed in the Electronic Appendix. Most of the data from this laboratory were generated with analytical spots 10–20 µm in diameter and a 2–5 nA current delivered to the sample surface, generating relatively intense secondary ion beam currents corresponding to $(2\text{--}5) \times 10^9$ c.p.s. for ¹⁶O, typical internal errors of $\leq \pm 0.15$ ‰ (1 standard error), and typical spot-to-spot precision on a nominally homogeneous material in a single grain mount of ~ 0.1 –0.2‰ (1σ). It should

be noted that the error of a single analytical spot arising from intra-analysis signal stability is described here as the ‘standard error’ or ‘s.e.’ of that spot; the standard deviation of a population of related analytical spots is described with the ‘ σ ’ symbol. All errors are given as 1 s.e. or 1σ unless otherwise noted.

A smaller subset of the data from this laboratory used analytical spots that were $5\ \mu\text{m}$ in diameter (1 nA), generating significantly weaker secondary ion beams (10^9 c.p.s. ^{16}O), resulting in larger internal errors of $\pm 0.25\%$ (1 s.e.). These data [reproduced from Eiler *et al.* (2007), but measured in the same session as many of the other data reported here] are inferior in quality to the rest of the data presented in this study. We present them to illustrate the sorts of measurements one might make on particularly small grains, inclusions, intracrystalline zonation features, or archived grains that were previously mounted in undesirable ways, and to document the sensitivity of our measurements to the details of sample preparation and analytical methods.

Finally, a subset of our data on synthetic olivines was generated using the CAMECA ims-7f geo in the Caltech Microanalysis Center. This single-collector, small-radius ion microprobe is capable of analyzing $^{18}\text{O}/^{16}\text{O}$ ratios in insulators with internal and spot-to-spot precisions of the order of $0.3\text{--}0.4\%$, 1σ , using a method of rapid peak hopping referred to as ‘pseudo multi-collection’. All measurements made with this instrument as part of this study used a $\sim 20\ \mu\text{m}$ primary beam ($\sim 2\text{--}3$ nA), generated secondary ion currents of the order of 1×10^9 c.p.s. for ^{16}O , and had typical internal errors of $\pm 0.2\%$, 1 s.e.

RESULTS

Tables 1–4 present all oxygen isotope measurements made as part of this study [some of which are reproduced from Eiler *et al.* (2007)], standardized as described above and in the Electronic Appendix.

Natural samples

Figure 1 presents histograms of the $\delta^{18}\text{O}_{\text{SMOW}}$ values of all *in situ* ion microprobe analyses of natural olivines and pyroxenes made for this study or compiled from previous publications (all were made on a single instrument—the CAMECA ims 1280—with a common set of methods and standards). All measurements have been normalized based on the average value observed for a concurrently analyzed SCO-3 intralaboratory olivine standard ($\delta^{18}\text{O}_{\text{VSMOW}}$ taken to equal 5.35%), as described in the Electronic Appendix. The gray band spanning the full height of the figure brackets the approximate range in $\delta^{18}\text{O}_{\text{SMOW}}$ of olivine in non-metasomatized mantle peridotites (Mattey *et al.*, 1994). The shorter, vertical heavy dashed lines indicate the average value for each population (i.e. the arithmetic mean of all measurements represented

by a given histogram in Fig. 1). The short, vertical heavy continuous lines indicate the $\delta^{18}\text{O}_{\text{SMOW}}$ values for bulk separates of that mineral in that sample, independently measured by fluorination (citations are provided below where data for each sample are discussed in detail). Finally, the horizontal heavy line in the upper right corner of this figure shows the average $\pm 2\sigma$ spot-to-spot reproducibility for bracketing standards analyzed in a single session on a single mount ($\pm 0.4\%$). Data for Batan peridotite xenolith olivines measured with a $5\ \mu\text{m}$ spot have approximately twice this error, and are indicated with shaded boxes. All samples of SCO olivine standard and Batan xenolith olivine measured on brass ‘bullets’ are indicated with a pattern of vertical lines within the relevant histogram box.

Relatively simple oxygen isotope distributions are observed for the San Carlos and S500-5b Koolau olivines. Both are consistent with normal (i.e. Gaussian) populations having standard deviations of $\sim 0.2\%$, 1σ —comparable with the average standard error for a single measurement. Measurements of SCO olivine made on brass bullets are noticeably broader in their distribution than the rest of the population, illustrating the importance of sample mounting for spot-to-spot precision. The San Carlos olivine served as an intralaboratory standard in this study, so these measurements provide no constraint on the accuracy of the technique. However, the average of ion microprobe analyses of S500-5b olivines (5.82%) is indistinguishable from the independently known value from laser fluorination measurements of olivine separates from the same sample (5.91% ; Wang, 2005), suggesting that the standardization scheme employed in this study is accurate.

The histogram for olivines from sample B3N [data reproduced from Eiler *et al.* (2007)] is relatively broad ($\pm 0.45\%$, 1σ), but is comparable with the spot-to-spot reproducibility for SCO standards on the same mount (Tables 1 and 3)—presumably because this brass ‘bullet’ mount has greater than ideal topography, and many of the measurements made of this sample employed a relatively small, low-intensity $5\ \mu\text{m}$ primary ion spot. These data present the clearest example of the importance of sample preparation and analytical method in achieving the highest external precision using secondary ionization mass spectrometry (SIMS) techniques for oxygen isotope analysis. The preparation and analytical approach to this sample was motivated by a desire to study rare, small melt inclusions (Eiler *et al.*, 2005), and we imagine future studies may be similarly driven to make such compromises. The data we present for this sample illustrate the challenges this approach will present to analytical accuracy and precision. We also note that sample B3N is a metasomatized peridotite containing a variety of secondary hydrous minerals and glass (Maury *et al.*, 1992; Eiler *et al.*, 2007),

Table 1: CAMECA ims 1280 analyses of San Carlos olivines

$\delta^{18}\text{O}_{\text{SMOW}}$	$\pm 1\text{s.e.}$	$\delta^{18}\text{O}_{\text{SMOW}}$	$\pm 1\text{s.e.}$	$\delta^{18}\text{O}_{\text{SMOW}}$	$\pm 1\text{s.e.}$	$\delta^{18}\text{O}_{\text{SMOW}}$	$\pm 1\text{s.e.}$	$\delta^{18}\text{O}_{\text{SMOW}}$	$\pm 1\text{s.e.}$
<i>R215-7.2 SCO-1</i>		<i>R215-7.2 SCO-2</i>		<i>S500-5b SCO-6</i>		<i>98M1 SCO-1</i>		<i>98M1 SCO-3</i>	
5-36	0-17	5-04	0-12	5-35	0-11	5-68	0-19	5-56	0-20
5-27	0-21	5-36	0-11	5-12	0-09	5-87	0-19	5-22	0-17
5-10	0-30	5-07	0-09	5-22	0-10	5-80	0-25	5-21	0-22
5-71	0-16	5-06	0-10	5-43	0-12	5-69	0-23	5-09	0-22
5-34	0-22	5-15	0-14	5-29	0-16	5-76 \pm 0-09		5-90	0-22
5-32	0-25	5-40	0-13	5-50	0-11	<i>98M1 SCO-2</i>		5-77	0-24
5-51	0-08	4-79	0-12	5-35	0-13	5-09	0-19	5-54	0-24
5-44	0-11	5-12 \pm 0-21		5-26	0-12	5-00	0-22	5-71	0-26
5-59	0-09	<i>Plug 3, hole 1 SCO</i>		5-31	0-14	4-84	0-19	5-13	0-17
5-06	0-12	5-22	0-24	5-31 \pm 0-11		5-10	0-25	5-37	0-22
5-15	0-09	5-20	0-25	<i>WI-STD19 SCO</i>		5-03	0-14	5-12	0-27
5-52	0-09	5-29	0-27	5-32	0-23	5-53	0-21	5-14	0-20
5-25	0-12	5-64	0-29	5-20	0-24	5-51	0-28	5-67	0-18
5-44	0-12	5-48	0-24	5-18	0-18	5-52	0-25	5-51	0-25
5-28	0-12	5-27	0-20	5-43	0-19	5-36	0-19	5-34	0-26
5-45	0-12	5-35 \pm 0-17		5-39	0-21	5-51	0-23	5-47	0-21
5-57	0-09	<i>S500-5b SCO-3</i>		5-26	0-18	5-22	0-18	5-13	0-22
5-65	0-08	5-55	0-16	5-74	0-25	5-09	0-23	5-38	0-34
5-49	0-14	5-60	0-13	5-31	0-20	4-85	0-28	5-52	0-23
5-42	0-11	5-53	0-29	5-39	0-20	5-28	0-18	5-26	0-28
5-77	0-12	5-56 \pm 0-04		5-44	0-26	4-92	0-24	5-15	0-21
5-52	0-09	<i>S500-5b SCO-4</i>		5-31	0-26	4-96	0-24	5-56	0-19
5-39	0-12	5-23	0-10	5-22	0-20	5-18 \pm 0-25		5-26	0-21
5-42 \pm 0-18		5-24	0-13	5-35 \pm 0-15		<i>B3N SCO-1*</i>		5-54	0-22
		5-28	0-15	<i>B3N SCO-2*</i>		6-03	0-23	5-40 \pm 0-23	
		5-25 \pm 0-02		4-98	0-22	6-57	0-22		
				4-30	0-25	5-56	0-23		
				4-86	0-24	5-16	0-26		
				4-71 \pm 0-36		5-83 \pm 0-61			

*Sample mounted in 5 mm bullet in a brass six-sample disk, rather than standard 1 inch polished mount; data from Eiler *et al.* (2007).

and so it is also possible that some variations within this sample are consequences of reaction between olivine and a metasomatic fluid. There are no obvious differences in major element composition or texture among the three grains analyzed from this sample (see electron probe data in the Electronic Appendix), although any distinguishing textural features could have been destroyed during sample preparation (they were studied as separate grain mounts, originally prepared for melt inclusion studies) and any differences in cation composition could have been erased by solid-state diffusion (which is faster for most cations than for O). The average of all ion microprobe analyses for sample B3N ($5.24 \pm 0.09\%$, 1 s.e. of the entire population of measurements) is within the range of olivines from

non-metamorphosed mantle olivines (i.e. the vertical gray band). It is lower than the value obtained by fluorination measurements of whole-rock powders of this sample using resistance-heated, sealed reaction vessels ($5.97 \pm 0.16\%$, implying a value for olivine of 5.6 to $5.7 \pm 0.2\%$; Fourcade *et al.*, 1994); this discrepancy may be a result of the inferior method of mounting used for sample B3N grains.

Olivine phenocrysts from Mauna Kea sample R215-7.2 exhibit the most pronounced variations seen in this study: a 2‰ range in $\delta^{18}\text{O}$ and a clearly non-Gaussian distribution. Most of the full range in $\delta^{18}\text{O}$ is observed in a single grain, R215-7.2 grain 2. Despite its large range and complex distribution in $\delta^{18}\text{O}$, the arithmetic mean of this population (4.64%) is indistinguishable from the value

Table 2: CAMECA ims 1280 analyses of R215-7.2, S500-5b and 98M1 olivines

$\delta^{18}\text{O}_{\text{SMOW}}$	$\pm 1\text{s.e.}$	$\delta^{18}\text{O}_{\text{SMOW}}$	$\pm 1\text{s.e.}$	$\delta^{18}\text{O}_{\text{SMOW}}$	$\pm 1\text{s.e.}$	$\delta^{18}\text{O}_{\text{SMOW}}$	$\pm 1\text{s.e.}$	$\delta^{18}\text{O}_{\text{SMOW}}$	$\pm 1\text{s.e.}$
<i>R215-7.2 grain 1</i>		<i>R215-7.2 grain 2, cont.</i>		<i>R215-7.2 grain 4</i>		<i>S500-5b OI-4</i>		<i>98M1 OI-D</i>	
4.99	0.26	4.74	0.11	5.20	0.13	5.85	0.10	4.52	0.26
5.22	0.23	5.31	0.09	5.44	0.12	5.94	0.14	4.32	0.29
4.60	0.20	4.55	0.10	4.66	0.11	5.84	0.13	4.21	0.18
4.98	0.30	4.49	0.10	4.49	0.12	6.06	0.11	4.54	0.18
4.90	0.23	4.49	0.11	4.41	0.10	6.05	0.15	4.40 \pm 0.16	
4.73	0.24	4.45	0.10	4.80	0.13	6.33	0.16	98M1 OI-E	
5.30	0.24	4.08	0.10	4.46	0.09	6.01 \pm 0.18		4.79	0.31
4.89	0.20	3.99	0.10	4.89	0.13	S500-5b OI-5		4.38	0.23
4.95 \pm 0.23		4.99	0.12	4.79 \pm 0.37		5.44	0.13	4.93	0.24
<i>R215-7.2 grain 2</i>		4.77	0.12	S500-5b OI-1		5.38	0.14	4.42	0.22
4.86	0.12	4.29	0.12	6.14	0.14	5.61	0.10	4.63 \pm 0.27	
4.66	0.13	4.27	0.15	5.96	0.13	5.39	0.12	98M1 OI-H	
4.77	0.12	4.71	0.11	5.79	0.12	5.45 \pm 0.11		4.01	0.20
4.66	0.11	3.62	0.10	5.99	0.11	98M1 OI-A		4.15	0.23
5.09	0.09	3.46	0.12	6.19	0.17	4.97	0.19	4.16	0.13
4.83	0.11	3.38	0.11	6.01 \pm 0.16		4.91	0.25	3.99	0.20
4.67	0.12	4.28	0.12	S500-5b OI-2		4.94 \pm 0.03		4.09 \pm 0.09	
4.93	0.14	3.84	0.15	5.71	0.12	98M1 OI-B		98M1 OI-G	
4.83	0.11	4.18	0.16	5.95	0.14	4.24	0.21	4.13	0.16
4.63	0.11	4.52	0.10	5.92	0.09	4.01	0.22	3.80	0.21
4.96	0.13	4.53	0.13	5.71	0.14	3.96	0.22	4.12	0.24
4.89	0.11	4.51	0.12	5.82 \pm 0.13		3.80	0.21	3.86	0.25
4.64	0.10	4.15	0.12	S500-5b OI-3		3.68	0.28	3.98 \pm 0.17	
4.67	0.12	4.55 \pm 0.45		5.54	0.18	3.94 \pm 0.21			
4.97	0.11			5.66	0.17	98M1 OI-C			
5.33	0.09			5.85	0.14	5.25	0.25		
4.93	0.10			5.60	0.09	5.27	0.21		
				5.66 \pm 0.14		5.26 \pm 0.01			

previously determined by laser fluorination for olivine separates from this rock (4.76‰; Eiler *et al.*, 1996). That is, as for sample S500-5b, our method of standardization appears to be accurate when samples are mounted and polished following recommended guidelines (Valley & Kita, 2009), even for distinguishing the relatively subtle (sub-per mil) oxygen isotope variations characteristic of fresh magmatic phases in mafic igneous rocks.

The bottom two histograms in Fig. 1 present oxygen isotope data for olivines and clinopyroxenes from Icelandic basalt 98M1. This sample was studied in two sessions—a first session that yielded highly aberrant results, which we speculated were due to topography on the sample surface; these data are not included in Fig. 1 or Table 2. The second session was performed after re-polishing the sample to create a flatter surface (although poorly hardened epoxy

precluded attaining relief less than 4 μm rather than the ideal $\leq 3 \mu\text{m}$). Only data from this second session are presented in Fig. 1. As for samples R215-7.2, S500-5b, and B3N, the average of measured $\delta^{18}\text{O}$ values of olivines from sample 98M1 is indistinguishable from the value determined for bulk olivine separates by laser fluorination [$4.34 \pm 0.09\%$, 1 s.e., of all ion probe measurements vs 4.53‰, respectively (Eiler *et al.*, 2001)]; it should be noted that laser fluorination measurements of olivine from this sample have relatively poor reproducibility ($\pm 0.2\%$, 1σ), suggesting intercrystalline heterogeneity]. Our ion microprobe analyses of the olivines in sample 98M1 are more variable in $\delta^{18}\text{O}$ than expected for analytical errors alone, and this principally reflects differences between grains (i.e. rather than zonation within single grains; Table 2 and Fig. 2). We discuss the systematics and possible causes of

Table 3: CAMECA ims 1280 analyses of B3N olivines and 98M1 clinopyroxenes

$\delta^{18}\text{O}_{\text{SMOW}}$	± 1 s.e.	$\delta^{18}\text{O}_{\text{SMOW}}$	± 1 s.e.	$\delta^{18}\text{O}_{\text{SMOW}}$	± 1 s.e.
<i>B3N Ol-1*</i>		<i>B3N Ol-3*</i>		<i>98M1 Px-A†</i>	
5.45	0.18	5.13‡	0.58	5.84	0.24
5.34	0.17	4.75‡	0.62	5.55	0.23
5.04	0.26	5.38‡	0.49	5.90	0.25
5.46	0.19	6.18‡	0.69	5.73	0.28
5.11	0.28	5.59‡	0.66	5.75 \pm 0.15	
5.09	0.24	5.27‡	0.46	<i>98M1 Px-B†</i>	
5.32	0.23	5.16‡	0.60	6.28	0.26
5.26 \pm 0.18		5.35 \pm 0.45		5.97	0.24
6.29‡	0.52			6.07	0.29
6.11‡	0.55			5.98	0.19
6.09‡	0.49			6.08 \pm 0.15	
5.87‡	0.62			<i>98M1 Px-C†</i>	
6.09 \pm 0.17				6.41	0.29
<i>B3N Ol-2*</i>				5.98	0.25
5.31‡	0.33			6.23	0.30
4.58‡	0.36			5.89	0.22
5.12‡	0.56			6.13 \pm 0.24	
5.04‡	0.40			<i>98M1 Px-D†</i>	
4.93‡	0.39			6.42	0.21
5.13‡	0.45			6.48	0.25
4.96‡	0.28			5.99	0.33
5.01 \pm 0.23				6.48	0.22
				6.34 \pm 0.24	

*Sample mounted in 5 mm bullet in a brass six-sample disk, rather than standard 1 inch polished mount.

†Accuracy estimated at $\pm 1\%$, owing to the potential for systematic uncertainties in matrix effect corrections.

‡Analysis made using a 5 μm spot, rather than the standard 10 μm spot.

It should be noted that B3N data are reproduced from Eiler *et al.* (2007).

these variations below. Pyroxene analyses in sample 98M1 yield a narrow range of $\delta^{18}\text{O}_{\text{SMOW}}$ values, $5.24 \pm 0.28\%$ (1σ , $n=16$). This value is significantly greater than that determined by laser fluorination ($4.69 \pm 0.03\%$, 1σ , Eiler *et al.*, 2001). This discrepancy between the averages from the two analytical techniques could be due to a greater than ideal distance of these grains from their mount center (although there is no obvious relationship of the $\delta^{18}\text{O}$ values to location, and similarly spaced olivines yielded accurate results); more probably, this discrepancy reflects the challenges of correcting for matrix effects in compositionally complex solid solutions such as pyroxene (Eiler *et al.*, 1997; Page *et al.*, 2010). Previous studies using the University of Wisconsin CAMECA ims-1280

Table 4: CAMECA ims 7f geo analyses of synthetic olivines

$\delta^{18}\text{O}^*$	± 1 s.e.	$\delta^{18}\text{O}^*$	± 1 s.e.
<i>MPDA-26 glass</i>		<i>MPDA-32 glass</i>	
0.01	0.14	0.16	0.21
-0.16	0.14	0.31	0.23
-0.63	0.11	-0.35	0.15
0.06	0.28	-0.65	0.17
0.17	0.15	0.53	0.24
0.04	0.15	0 \pm 0.49	
-0.46	0.16	<i>MPDA-32 olivine</i>	
0.56	0.15	0.42	0.15
0.35	0.15	-0.40	0.18
0.25	0.23	0.22	0.17
-0.20	0.19	-0.25	0.17
0 \pm 0.35		0 \pm 0.39	
<i>MPDA-26 olivine</i>			
0.01	0.16		
-0.10	0.16		
0.28	0.23		
0.13	0.14		
0.13	0.14		
-0.45	0.18		
0 \pm 0.25			

* $\delta^{18}\text{O}$ values for glass and olivine are separately normalized to an average of 0‰.

demonstrate that olivines spanning a range in forsterite content comparable with common terrestrial igneous and mantle rocks exhibit indistinguishable instrumental mass fractionations using the instruments and conditions employed in this study, whereas pyroxenes exhibit a large ($\sim 5\%$ from En to Wo) range in instrumental mass fractionation (Valley & Kita, 2009). We have attempted to correct for this effect by comparing the Ca contents of pyroxenes in sample 98M1 with the correlation between Ca content and instrumental fractionation for standard pyroxenes (Valley & Kita, 2009; see the Electronic Appendix for further details). However, this correlation is demonstrably non-linear and only sparsely defined. It probably cannot be applied with confidence better than an estimated ~ 0.3 – 0.5% . This discrepancy will have to be resolved with future work.

The isotopic distributions documented in Fig. 1 reflect a combination of intra- and intercrystalline variations within samples and differences in bulk composition between samples. The differences in average $\delta^{18}\text{O}$ between samples considered in this study are generally within

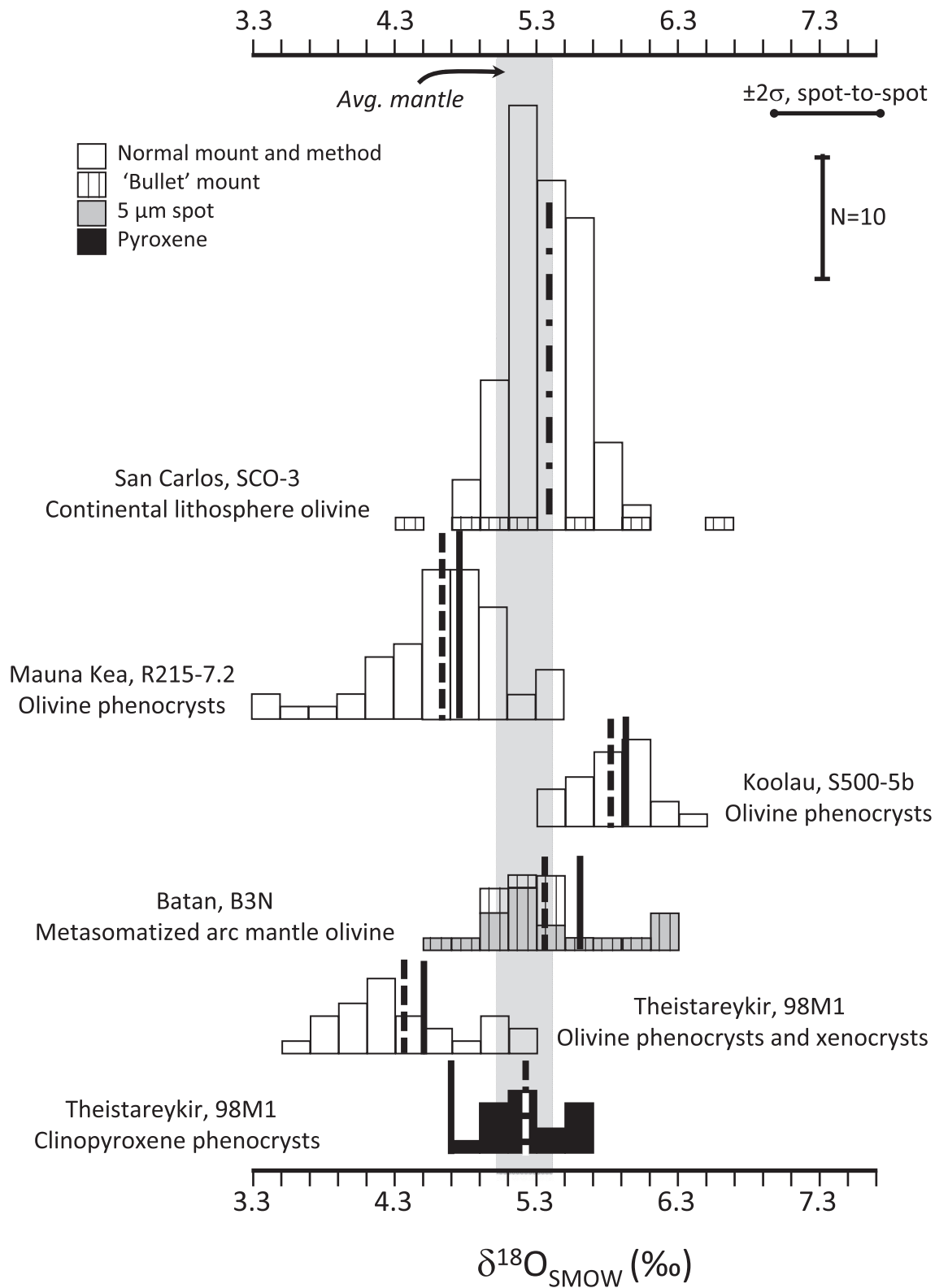


Fig. 1. Histograms showing the distribution in $\delta^{18}\text{O}$ values of the natural olivines and pyroxenes examined in this study. The vertical bar in the upper right corner provides the scale for numbers of analyses in each data bin. The horizontal bar in the upper right corner illustrates the typical external (spot-to-spot) error, 2σ , for measurements made on the Cameca ims-1280 with the techniques employed in this study (Valley & Kita, 2009). Unfilled boxes are measurements of olivine made with a $10\ \mu\text{m}$ spot on samples mounted and polished following the

(continued)

error of those previously observed by fluorination studies of milligram-sized aliquots of the same samples. Therefore, it seems likely that $\sim 1.5\%$ of the range we observe among minerals (i.e. roughly half of the full range) reflects differences in $\delta^{18}\text{O}$ between the magmas from which those minerals grew. This interpretation assumes, however, that there are no non-equilibrium fractionations associated with olivine and pyroxene growth that are shared by most or all olivines from each sample.

Figure 2 illustrates the contribution of intercrystalline variability within a single hand sample to the overall variability of the dataset. The histogram shows the difference between the average $\delta^{18}\text{O}$ of each grain and the average $\delta^{18}\text{O}$ of all grains of the same mineral (olivine or pyroxene) from the same sample, analyzed in the same mount. Three groups of data are distinguished. Most (20) grains for which this comparison can be made are part of a distribution that has a generally Gaussian shape and a standard deviation of $\pm 0.20\%$ (1σ). This is comparable with the internal errors of our measurements, and we suggest that these grains come from samples that exhibit little or no intercrystalline oxygen isotope variability (this includes sample R215-7.2, which exhibits pronounced intracrystalline zonation in at least one grain, but no significant differences between average values for each grain). Four grains were analyzed in a brass mount (vertically ruled boxes), and some of these include measurements made with small ($5\ \mu\text{m}$) analytical spots; these exhibit greater grain-to-grain variability, but this plausibly reflects the decreased precision of these measurements. Finally, the seven grains of olivine from sample 98M1 (stippled boxes) were mounted and analyzed using recommended methods, but yielded a broad range of grain averages. These grains are generally internally homogeneous (Table 2, and discussion below), and their sample average is indistinguishable from that for the fluorination analysis of olivine in this sample, so we interpret this as true intercrystalline variability. This conclusion is consistent with the relatively poor reproducibility of laser fluorination measurements of grain separates from this sample (Eiler *et al.*, 2001).

The inset to Fig. 2 plots the average $\delta^{18}\text{O}$ value vs the magnesium number [i.e. molar $\text{Mg}/(\text{Mg} + \text{Fe})$] for the olivines from 98M1, revealing that the two highest $\delta^{18}\text{O}$ grains are the most forsteritic (Mg-number ~ 0.910 – 0.915), whereas the five lower $\delta^{18}\text{O}$ grains are part of a population

that exhibits a negative correlation between $\delta^{18}\text{O}$ and Mg-number. All seven of these grains are relatively calcium rich (0.3 – 0.4 wt % CaO) and they form a continuous trend in plots of Mg-number vs wt % NiO and vs wt % Cr_2O_3 (see the Electronic Appendix for electron microprobe data), so we infer that all are phenocrysts related to their host lavas (i.e. rather than mantle xenocrysts). A full understanding of these data would require study of more samples related to 98M1, but previous studies of the geochemistry of Icelandic lavas suggest the action of processes that could explain our observations. Basalts from Theistareykir are products of magma mixing, and are suspected of having been contaminated by low- $\delta^{18}\text{O}$ crustal assimilants (as is common for Icelandic lavas generally), and are variably differentiated (Eiler *et al.*, 2001, and references therein). We suggest that the data array in Fig. 2 could be understood if the highest $\delta^{18}\text{O}$, most magnesian olivines are phenocrysts that grew from primitive melts prior to contamination; subsequently a low- $\delta^{18}\text{O}$ assimilant was added soon after the olivines grew, and the resulting contaminated magma underwent fractional crystallization (perhaps accompanied by mixing with fresh primitive melt), gradually increasing in $\delta^{18}\text{O}$ with further differentiation, as is known to occur during fractionation of basaltic magmas (Eiler, 2001). Magma mixing during or prior to eruption intermingled the crystals grown throughout this history to create the complex and variable population found in 98M1. Regardless of whether this hypothesized scenario is correct in its particulars, the systematic variations of $\delta^{18}\text{O}$ and mineral chemistry we observe suggest that future oxygen isotope studies of Icelandic lavas on a microscale could provide valuable insights into their origin and evolution.

Figure 3 further isolates the component of intracrystalline variability in the suite of samples examined in this study by presenting a histogram of the differences between each analyzed point and the average for all analyzed points from the grain in which that point was measured. The resulting distribution is half the width of the distribution of all $\delta^{18}\text{O}$ values prior to this grain-by-grain normalization, and most of the data are within a much narrower range of $\pm 0.4\%$, indicating that only a small fraction of the variations in Fig. 1 represent intracrystalline zonation. Figure 3 contains an overlay of a curve illustrating a Gaussian distribution having a standard deviation equal

Fig. 1. Continued

recommendations of Valley & Kita (2009; although it should be noted that some spots are more than 5 mm from the mount center) and have typical internal errors of $\sim 0.1\%$, 1 s.e., and spot-to-spot reproducibility of $\sim 0.2\%$, 1σ . Gray filled boxes are measurements of olivine made with a $5\ \mu\text{m}$ spot, and have typical external errors of $\sim 0.25\%$, 1 s.e. and spot-to-spot reproducibility of $\sim 0.5\%$, 1σ . Unfilled or gray boxes having vertical bars were made on a sample mounted in a 5 mm brass 'bullet' held in a 1 inch brass cylinder. Black filled boxes are measurements of clinopyroxene made with a $10\ \mu\text{m}$ spot. All measurements of olivine were standardized against a concurrently analyzed San Carlos olivine standard. Dashed heavy lines mark the arithmetic mean of each population. Continuous heavy lines mark the independently known bulk $\delta^{18}\text{O}$ of mineral separates from the same rock, from laser or conventional fluorination studies (see text for references). The light gray vertical band extending across all the histograms indicates the typical range of $\delta^{18}\text{O}$ values for mantle olivines (Mattey *et al.*, 1994).

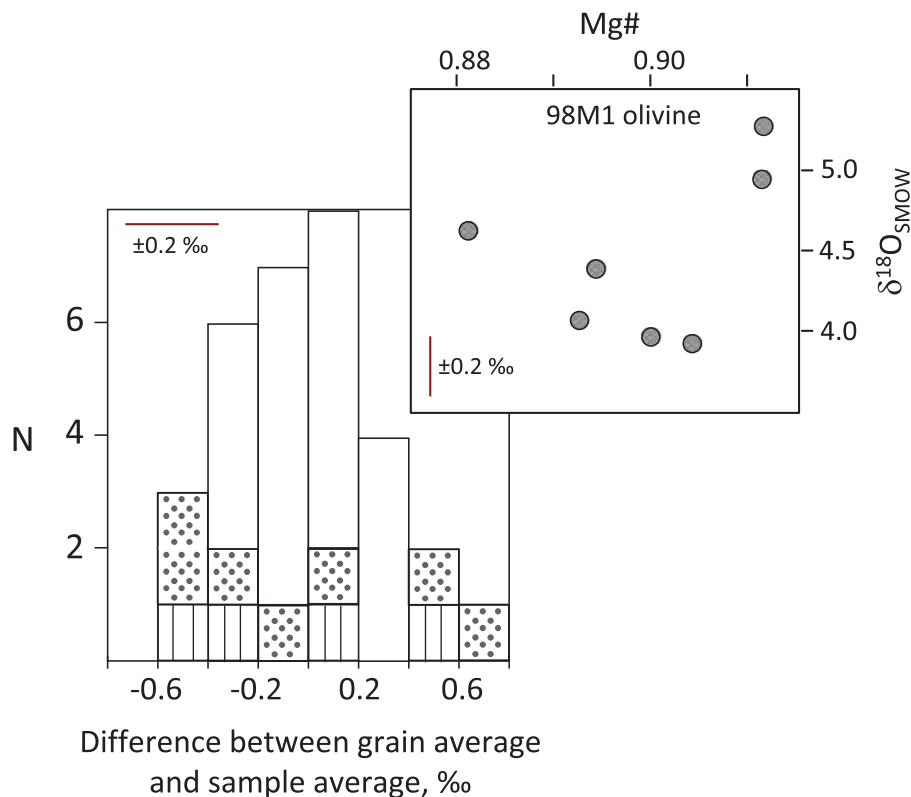


Fig. 2. Histogram showing the difference between the average $\delta^{18}\text{O}$ of a single grain and the average $\delta^{18}\text{O}$ for all grains of that same mineral from the same rock in the same mount (in ‰). A value is presented only if two or more grains of the same mineral from the same sample were analyzed in a single mount (thus only 31 of the 34 grains analyzed in this study appear in this figure). Unfilled boxes show data measured with a large analytical spot on ideally prepared sample mounts for San Carlos olivine, R215-7.2 olivine (Mauna Kea), S500-5b olivine (Koolau) or 98M1 pyroxene (Iceland). Vertically ruled boxes depict data for San Carlos olivine and B3N olivine (Batan) analyzed in a copper bullet mount and/or using a small ($5\ \mu\text{m}$) analytical spot. Stippled boxes depict data for olivines from 98M1 (Iceland). The inset compares the average $\delta^{18}\text{O}$ values with average magnesium numbers for olivine grains from 98M1.

to the average external (point-to-point) analytical error of each spot (estimated $\pm 0.2\%$, 1σ). Most of the observed distribution is consistent with the expected results if the measured grains are homogeneous in $\delta^{18}\text{O}$. The exceptions are the ~ 15 analytical spots that make up the longer than expected ‘tails’ to the measured distribution, extending beyond the calculated Gaussian curve. Measurements made with a $5\ \mu\text{m}$ spot or on a ‘bullet’ style mounting (gray filled or vertically ruled boxes in Fig. 3) are noticeably broader in their distribution than the rest of the measurements, again illustrating the importance of sample preparation and analytical method in high-precision ion microprobe analyses. Clinopyroxene in sample 98M1 appears unanomalous in this figure; presumably because it lacks intracrystalline zonation, independent of whatever problems might exist with the accuracy of our matrix corrections for this phase.

Figure 4 shows the intracrystalline variations in $\delta^{18}\text{O}$ that we observe re-normalized in yet another way. Here, we present a histogram showing the distribution of

intracrystalline standard deviations in $\delta^{18}\text{O}$, again compared with the expected distribution if all variations reflected analytical errors in measurements of a homogeneous population (bell-shaped curve; it should be noted that this is an approximation because it assumes a typical number of measurements per grain, taken to be eight). Most grains are part of a broadly normal distribution centered on an average error similar to our estimate of the point-to-point external errors (both are $\pm 0.2\%$). Only about five grains are exceptions to this distribution, and only one, R215-7.2 grain 2, is a clear exception to this normal distribution (the second grain with a point-to-point reproducibility of 0.37 is sufficiently close to the predicted Gaussian curve that we are less sure it represents true intracrystalline heterogeneity). The normalized χ^2 value of this entire population is 4.9. We conclude that not only are there few single analytical spots that differ from their grain averages by more than expected by analytical error alone (Fig. 3), but also those exceptions are not randomly distributed among all grains; rather, they

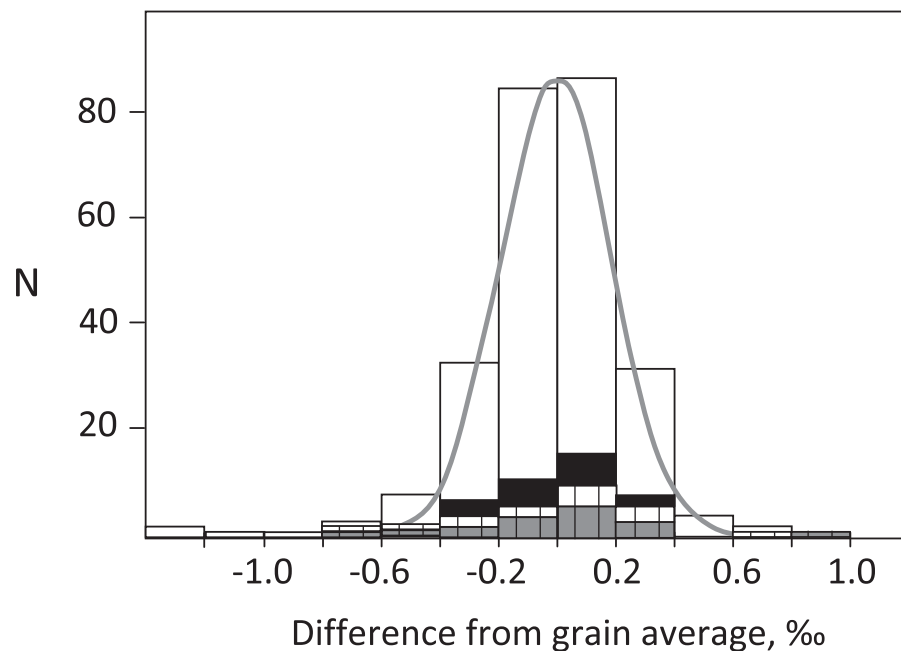


Fig. 3. Histogram illustrating the intracrystalline variability in $\delta^{18}\text{O}$ for all grains analyzed in this study. Each value included in this histogram is a single *in situ* measurement of $\delta^{18}\text{O}$ in a grain, normalized to the average for all *in situ* measurements of $\delta^{18}\text{O}$ in that grain (i.e. by definition, all measurements in one grain average to zero). Gray filled boxes are measurements of olivine made with a $5\ \mu\text{m}$ spot. Gray or white boxes with vertical bars were made on a sample mounted in a 5 mm brass 'bullet' held in a 1 inch brass cylinder. The black boxes represent data for 98M1 pyroxenes. The continuous gray curve illustrates a Gaussian distribution having a width consistent with a $1\ \sigma$ error of $\pm 0.2\text{‰}$ (the nominal spot-to-spot precision of our analyses using the preferred beam conditions and sample preparation methods). It should be noted that only a small fraction of all points measured with a $10\ \mu\text{m}$ spot on a sample prepared according to the recommendations of Valley & Kita (2009) differ from their respective grain averages by more than expected for a homogeneous material given the analytical precision of the measurements.

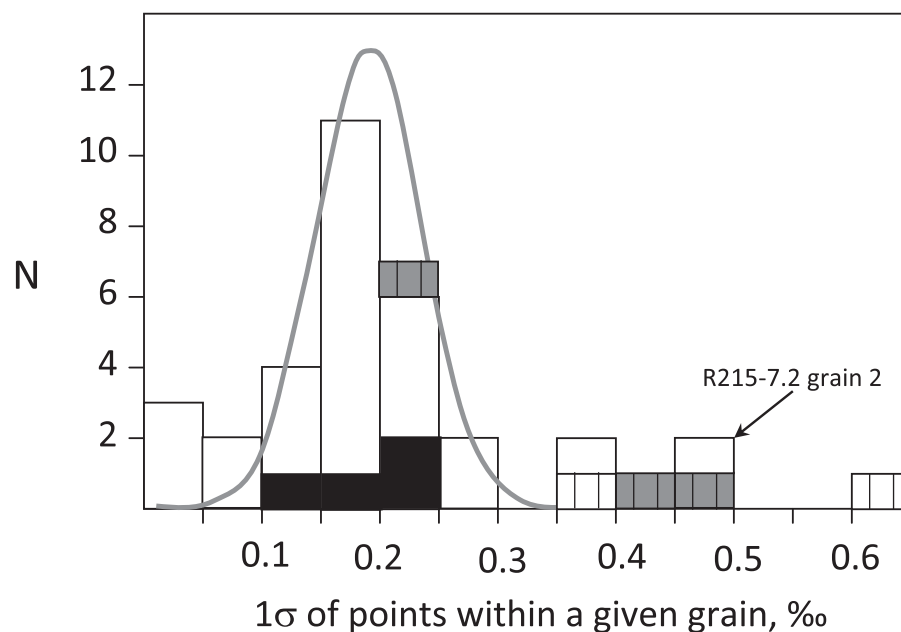


Fig. 4. Distribution of intragrain standard deviations for all single grains analyzed in this study. Gray filled boxes are grains studied using a less precise $5\ \mu\text{m}$ spot. Gray or white boxes with vertical bars were made on a sample mounted in a 5 mm brass 'bullet' held in a 1 inch brass cylinder. The black boxes represent data for pyroxenes from sample 98M1. The thick gray curve marks the expected distribution of standard deviations assuming an average analytical error of $\pm 0.2\text{‰}$ and a typical population of eight spots per grain. Only one grain, R215-7.2 grain 2, mounted according to the recommendations of Valley & Kita (2009) and analyzed with a $10\ \mu\text{m}$ spot, exhibits a standard deviation substantially higher than expected for a homogeneous material given the analytical precision of the measurements.

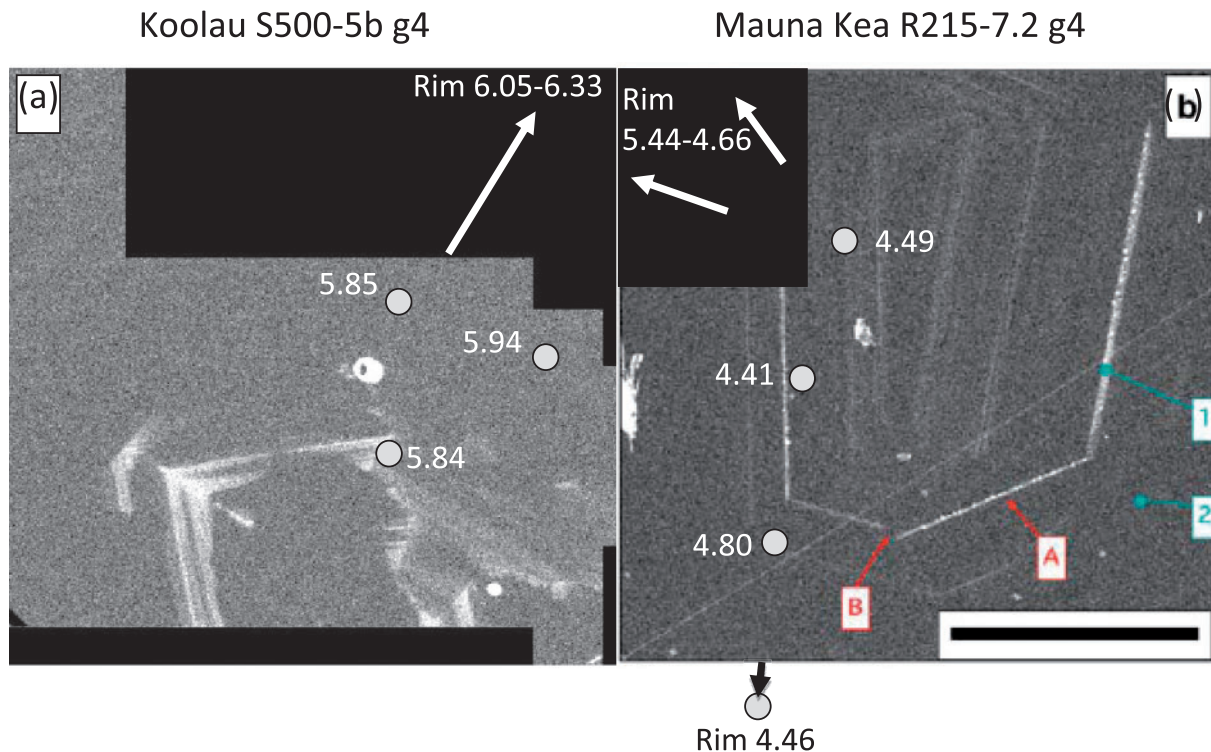


Fig. 5. Maps of phosphorus distribution measured by wavelength-dispersive spectroscopic (WDS) analysis on a JEOL electron microprobe for two representative natural olivine grains that exhibit variations in $\delta^{18}\text{O}$ consistent with homogeneous distributions: (a) grain 4 of Koolau basalt S500-5b; (b) grain 4 of Mauna Kea basalt R215-7.2. These maps are reproduced with permission from Milman-Barris *et al.* (2008) [it should be noted that inset labels, 'A', 'B', '1' and '2' in (b) refer to features discussed in that paper but not specifically discussed here]. The field of view for each image is $\sim 250\ \mu\text{m}$ [the black bar at the lower right corner of (b) is $100\ \mu\text{m}$ long]. Brighter pixels are richer in P than darker pixels. Values of $\delta^{18}\text{O}_{\text{SMOW}}$ and locations of spots analyzed within the field of view of the P maps are indicated; arrows point in the direction of additional points analyzed outside the field of view (all of these additional points lie within $\sim 30\ \mu\text{m}$ of a grain edge).

preferentially occur in an even smaller proportion of exceptionally heterogeneous grains. Furthermore, it is clear that $\sim 1\%$ and smaller intracrystalline isotopic variations can be studied reliably only by using the most precise, large spot size (and thus high-current) analytical conditions on samples prepared to achieve a suitably flat, smooth surface.

In summary, the data presented in Figs 1–4 demonstrate that olivines and pyroxenes from basalts and peridotites, at least as represented by our sampling of several dozen grains from five rocks, are generally internally homogeneous in $\delta^{18}\text{O}$ to within $\sim 0.2\%$, even in samples with large (multiple per mil) intercrystalline and intersample variations (this is even true of grains that exhibit noticeable major element intracrystalline zonation; e.g. several grains from sample S500-5b; Electronic Appendix Table 1). Although this result could have several interpretations (particularly given the small number of samples we have studied), it is consistent with the notion that oxygen isotope variations between minerals in mafic lavas and peridotites mostly reflect isotopic contrasts between primitive magmas (and their sources), changes in $\delta^{18}\text{O}$ of

magmas over time and length scales larger than those typically sampled by a single crystal, and possibly contrasts between the peridotites and the metasomatic agents with which they react. These variations are not typically expressed at the scales of single grains, presumably because minerals in these systems generally grow in or close to isotopic equilibrium with surrounding melts and/or fluids over time scales and length scales shorter than those of magmatic isotopic variations. The clearest exception to this generalization seen in this study is grain 2 from Mauna Kea lava R215-7.2; this sample is explored in further detail below.

Figure 5 shows maps of the P distributions in two grains (modified from Milman-Barris *et al.*, 2008) that are either homogeneous in oxygen isotope ratio within the limits of our analyses (grain 4 from Koolau basalt S500-5b; $\delta^{18}\text{O}_{\text{SMOW}} = 6.01 \pm 0.18\%$, $n = 6$) or vary by only a small multiple of the analytical precision (grain 4 from Mauna Kea basalt R215-7.2; $\delta^{18}\text{O}_{\text{SMOW}} = 4.79 \pm 0.37\%$, $n = 8$). Oxygen isotope measurements made within the field of view of the P map for each sample are indicated, as are the directions toward additional measurements

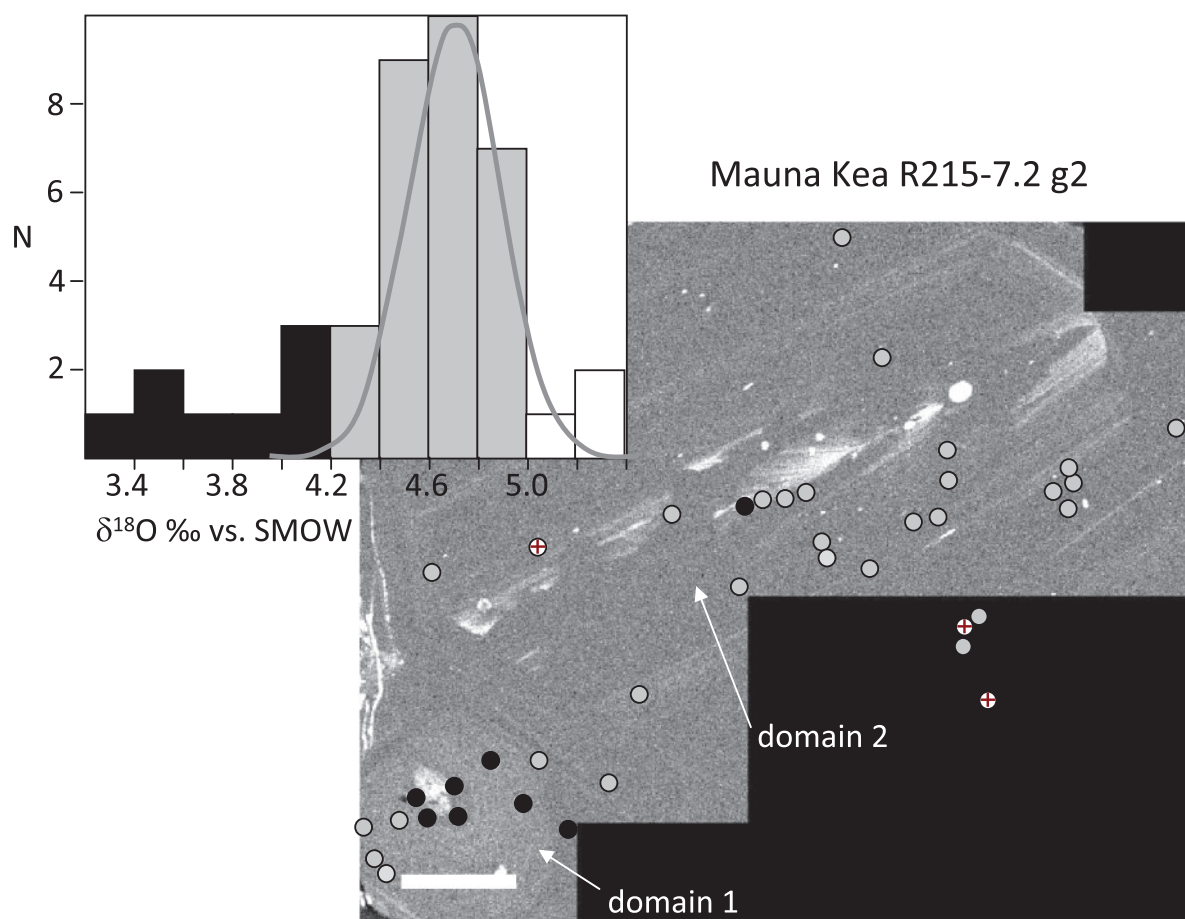


Fig. 6. Map of the phosphorus distribution, measured by WDS analysis on a JEOL electron microprobe, for grain 2 of Mauna Kea basalt R215-7.2. This map is reproduced with permission from Milman-Barris *et al.* (2008). The field of view is ~ 1 mm (the white bar at the lower left corner is $100\ \mu\text{m}$ long). Brighter pixels are richer in P than darker pixels. The two subgrains of this glomerocryst ('domain 1' and 'domain 2') are indicated. Locations of spots analyzed within the field of view of the P maps are indicated by circles; black filled circles correspond to low- $\delta^{18}\text{O}$ spots ($<4.2\text{‰}$ vs SMOW), gray circles have $\delta^{18}\text{O}$ values between 4.2 and 5.2‰ , and white circles containing a cross correspond to high- $\delta^{18}\text{O}$ spots ($>5.2\text{‰}$ vs SMOW). The inset histogram shows the distribution in $\delta^{18}\text{O}$ of single spots analyzed on this grain, shaded to distinguish relatively low- and high- $\delta^{18}\text{O}$ spots (black and white, respectively; these are the populations of black and white spots plotted on the P map).

outside the area of the P map (generally on the rims of these equant, millimeter-sized grains). Both of these grains fractured and partially fell out of their mounting medium after analysis, and one (R215-7.2 grain 4) was re-polished before the analytical spots could be re-imaged. Therefore, the locations of the analytical spots are best estimates based on the x - y coordinates of measurements in the instrument reference frame and pre-analysis images of the samples. We estimate that they have uncertainties of up to tens of micrometers. Although we have produced only a small number of such P maps for grains that have been analyzed for oxygen isotope composition, they demonstrate that the processes of non-equilibrium growth responsible for oscillatory P zonation (visible in R215-7.2 grain 4), and skeletal growth and P-poor resorption features (visible in S500-5b grain 4), can occur without large (i.e. per-mil amplitude) oxygen isotope variations. We

cannot confidently state whether or not these P zonation patterns are associated with subtle (a few tenths per mil or less) oxygen isotope variations, but it is clear that whatever causes these features it is not principally responsible for the $\sim 3\text{‰}$ range in $\delta^{18}\text{O}$ seen in our dataset as a whole (Fig. 1). Although this result could have several possible interpretations, a relatively straightforward one is that non-equilibrium P enrichments in olivine, whether caused by diffusion-limited P enrichments in the melt adjacent to the growing grains (Watson & Muller, 2009) or non-equilibrium partitioning at the melt-grain interface (Watson, 1996), can occur in systems that maintain or closely approach oxygen isotope exchange equilibrium between melt and the growing crystal.

Olivine grain 2 from Mauna Kea lava R215-7.2 differs from the two olivines described above. As shown in Fig. 6, it spans a range in $\delta^{18}\text{O}$ from 3.38 to 5.33‰ —nearly

twice the range found in fresh olivines from most terrestrial basalts by laser fluorination techniques (Eiler, 2001, and references therein), and $10\times$ the analytical precision of the ion microprobe technique used in this study. It should be noted that despite its large range, the average $\delta^{18}\text{O}_{\text{SMOW}}$ value for this grain (4.55‰) is similar to the value determined for olivine separates from the same rock using laser fluorination (4.76‰; see Fig. 1). Figure 6 presents an X-ray map of the P distribution in this grain, with an overlay indicating the locations of oxygen isotope measurements made on it, indicating spots that are low in $\delta^{18}\text{O}_{\text{SMOW}}$ (<4.2‰; black circles), part of the main population (between 4.2 and 5.2‰; gray circles) or have values higher than 5.2‰ (white circles with a cross). The inset to Fig. 6 depicts the histogram of all $\delta^{18}\text{O}$ values for this grain. Analytical spots on this grain are confidently located because the ion probe pits were clearly visible in the P map, which was generated after the oxygen isotope measurements were made. It should be noted that some bright spots in Fig. 6 are locations of ion beam marks on the sample surface made while centering the beam prior to measurements; these are obvious because no corresponding black, gray or white, cross-filled circle overlies them.

Most analytical spots in grain R215-7.2 grain 2 [a glomerocryst assembled from a small sub-grain ('domain 1') and a large sub-grain ('domain 2')] span a relatively narrow range in $\delta^{18}\text{O}_{\text{SMOW}}$ (4.2–5.2‰) consistent with a single value of $\sim 4.8\text{‰}$. The low- $\delta^{18}\text{O}$ domains (<4.2‰) are texturally associated with (inside or adjacent to) two features revealed in the P map of this grain: the lowest $\delta^{18}\text{O}$ values are within or adjacent to an irregularly shaped P-rich core of the small sub-grain in the lower left corner of Fig. 6; and a group of low $\delta^{18}\text{O}$ values, including one below 4.2‰, is located in or near a band of P-rich olivine running down the center of the larger sub-grain. This P-rich band exhibits a peculiar oscillatory texture described as 'feathery' by Milman-Barris *et al.* (2008), who suggested that it is related to non-equilibrium P entrapment during rapid crystal growth.

The data shown in Fig. 6 suggest that anomalously low $\delta^{18}\text{O}$ values in grain R215-7.2 grain 2 are associated with regions of P enrichment. If so, this could provide an important clue to the mechanisms responsible for this grain's pronounced intracrystalline isotopic zonation. However, the ion microprobe analyses of $\delta^{18}\text{O}$ were made at a scale of $\sim 10\ \mu\text{m}$, whereas P concentrations commonly vary over $\sim 1\ \mu\text{m}$ length scales in olivine phenocrysts (Milman-Barris *et al.*, 2008). Therefore, the association of P with low $\delta^{18}\text{O}$ in Fig. 6 is suggestive but not definitive. To explore this relationship further, subsequent to both the X-ray mapping and *in situ* oxygen isotope study of this grain, we used the NanoSIMS 50L high-spatial-resolution ion microprobe to determine the P content of olivine in the

Table 5: $^{31}\text{P}^-/^{30}\text{Si}^-$ ratios of R215-7.2 grain 2 olivine

$^{31}\text{P}^-/^{30}\text{Si}^-$	± 1 s.e. (%)	$\delta^{18}\text{O}_{\text{SMOW}}^*$
0.00327	0.75	4.62
0.00341	0.50	4.83
0.01159	0.29	4.63
0.01907	0.20	4.11
0.00297	0.47	4.73
0.00291	0.54	4.93
0.00354	0.42	4.24
0.00309	0.43	4.47
0.00767	0.34	4.49
0.00325	0.41	4.49
0.00303	0.53	4.25
0.00301	0.52	4.89
0.00361	0.50	4.93
0.00434	0.40	4.85
0.00256	0.64	4.95
0.00288	0.62	4.67
0.00285	0.55	5.30
0.00276	0.54	4.90
0.01637	0.21	3.34
0.01672	0.22	4.14
0.00070	San Carlos olivine (0.012 wt % P_2O_5)	

*From Table 2.

center-bottom of 19 of the pits left by oxygen isotope analyses in this sample (including five of those that are markedly low in $\delta^{18}\text{O}$), so that we could confidently compare the P and $\delta^{18}\text{O}$ variations (see the Electronic Appendix for details regarding the analytical method). Table 5 and Fig. 7 summarize the results of these analyses. We find that low- $\delta^{18}\text{O}$ spots in this sample are generally P enriched relative to the bulk grain, and the highest P spots are the lowest in $\delta^{18}\text{O}$ (although it should be noted that some spots with normal P contents are measurably lower in $\delta^{18}\text{O}$ than the grain average). These data reinforce the suggestion from Fig. 6 that low $\delta^{18}\text{O}$ is associated with P enrichment.

In a previous study of P in olivines, Milman-Barris *et al.* (2008) concluded that concentrations in excess of those expected for equilibrium partitioning with respect to the coexisting melt result from non-equilibrium mechanisms of phenocryst growth, such as diffusion-limited enrichment of incompatible elements near the surfaces of growing crystals (Watson & Muller, 2009) or 'surface entrapment' (i.e. relative compatibility of trace elements in sites specific to mineral surfaces; Watson, 1996). Thus, our finding that low $\delta^{18}\text{O}$ values can be associated with P enrichments in

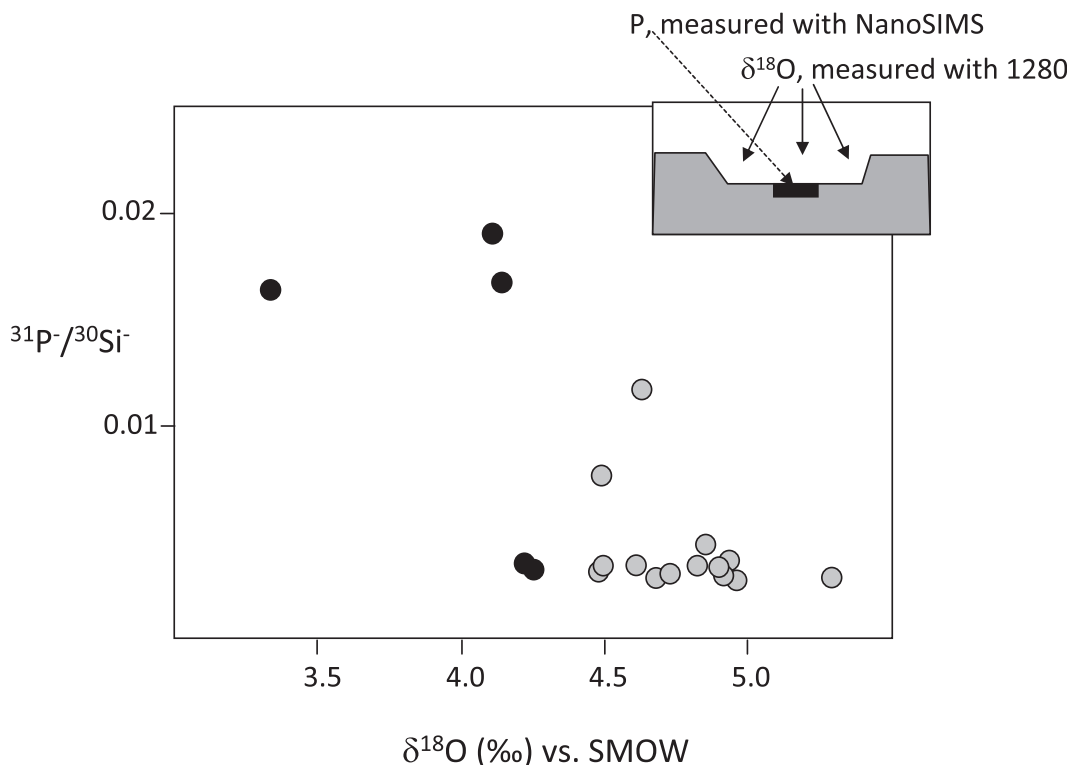


Fig. 7. Comparison of $\delta^{18}\text{O}$ values with measured $^{31}\text{P}/^{30}\text{Si}^-$ ion intensity ratios (inferred to be proportional to P concentration; Table 5) for Mauna Kea sample R215-7.2 grain 2. Oxygen isotope measurements were made by CAMECA ims 1280 ion microprobe, whereas $^{31}\text{P}/^{30}\text{Si}^-$ ratios were measured by CAMECA NanoSIMS 50L ion microprobe. Analyses are from very nearly the same site, as illustrated in the inset. All spots appearing in this figure are among the population of spots illustrated in Fig. 6. Black filled circles correspond to $\delta^{18}\text{O}$ values $< 4.2\text{‰}$ (vs SMOW), as in Fig. 6.

some olivines raises the possibility that melt–phenocryst oxygen isotope fractionations could be similarly influenced by one or both of these non-equilibrium partitioning processes. For example, let us consider the case in which P enrichments in olivine are caused by diffusion-limited enrichment of P (which is incompatible and slowly diffusing) in the melt adjacent to the growing crystal surface. If the growth rate of that olivine were controlled by melt-phase diffusion of some limiting reactant, such as MgO , to the crystal surface, the crystal could preferentially incorporate ^{16}O because Mg^{16}O will diffuse faster, and therefore feed the growing surface with a proportionately higher flux than Mg^{18}O . If this or some other kinetic fractionation occurred in natural magma, it would constitute an important revision to our understanding of oxygen isotopes in igneous systems, which are generally assumed to conform to local equilibrium during melting and crystallization. Below we explore this hypothesis in more detail by study of experimentally grown olivines.

Synthetic samples

Previous studies of P distributions in igneous olivines (Milman-Barris *et al.*, 2008; McCanta *et al.*, 2009) included

experiments in which olivines were grown from synthetic basaltic melts during cooling at controlled rates. Such materials are useful for our purposes for two reasons: they involve growth in a closed system, where the oxygen isotope ratios of olivines will be controlled by partitioning with respect to the parent melt (i.e. as opposed to some external reservoir, such as a buffering gas); and the product olivines exhibit a range of textures and patterns of P enrichment, including both oscillatory zonation (which we found can exist in the absence of oxygen isotope variations; Fig. 5) and skeletal and other complex zonation patterns (which we have found associated with large oxygen isotope variations; Fig. 6). We examined two experimental charges to determine whether P zonation in the olivines they contain is associated with oxygen isotope variations of the amplitude observed in sample R215-7.2 grain 2 (i.e. $\sim 2\text{‰}$).

Figure 8a and c shows P maps and *in situ* oxygen isotope measurements for olivines from experiments MPDA-26 and MPDA-32, which were performed following experimental protocols similar to those of Milman-Barris *et al.* (2008) and McCanta *et al.* (2009). The P maps were produced by X-ray mapping (as in Figs 5 and 6); the oxygen

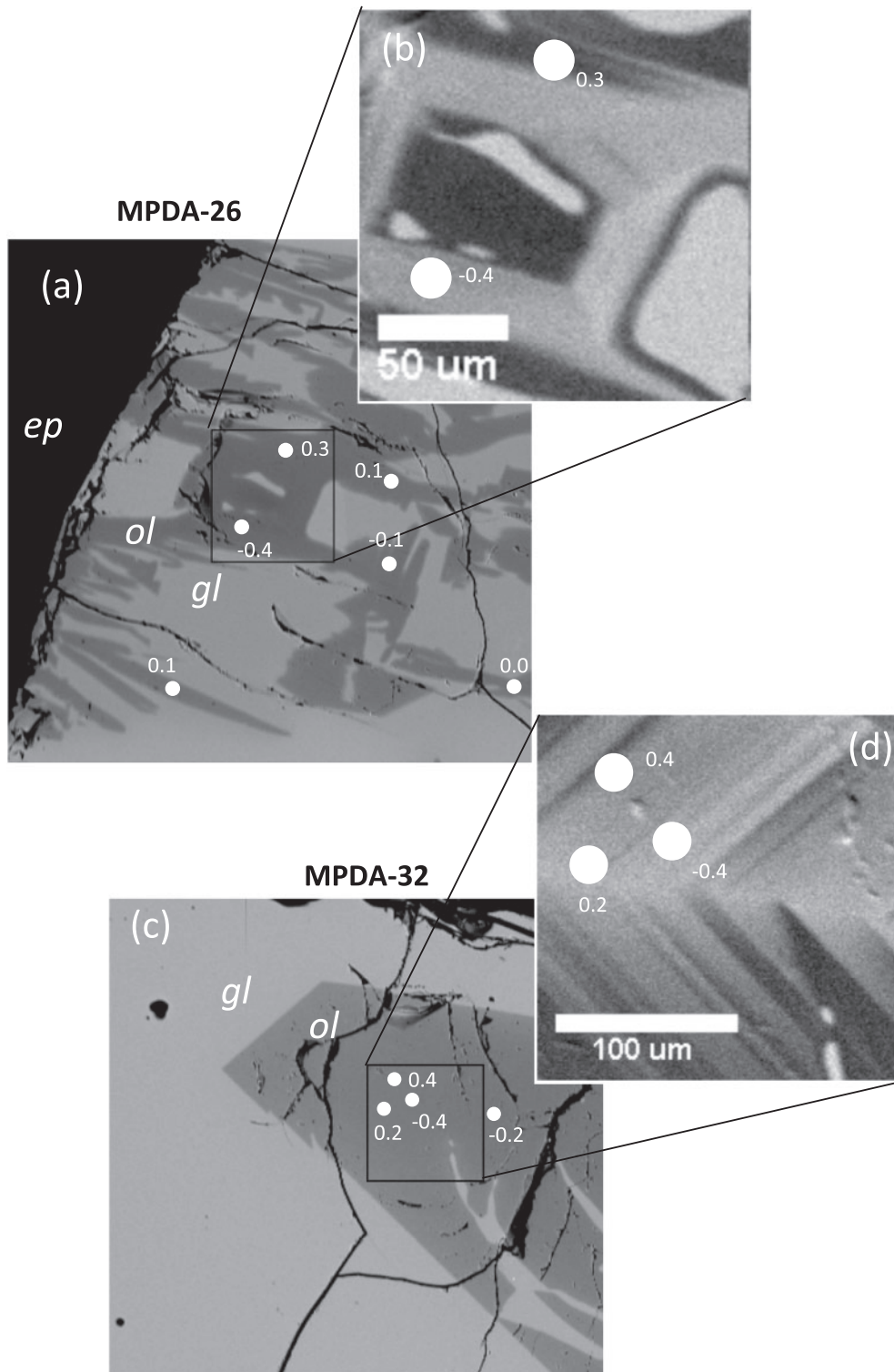


Fig. 8. Maps of backscattered electron intensity (a and c; measured by SEM; gl, glass; ol, olivine; ep, epoxy) and the phosphorus distribution (b and d; measured by WDS analysis on a JEOL electron microprobe), for two synthetic aggregates of olivine and basaltic glass. Both are products of controlled cooling experiments in which basaltic melt was heated to 1280°C (above its liquidus temperature) and then cooled at controlled rates of 30°C h⁻¹ (for experiment MPDA-26; a and b) or 1°C h⁻¹ (for experiment MPDA-32; c and d). These maps are from McCanta *et al.* (2009). White scale bars are provided in (b) and (d); (a) is ~500 μm wide and (c) is ~750 μm wide. Brighter pixels in (b) and (d) are richer in P than darker pixels. Locations of spots analyzed within the field of view of the P maps are indicated by circles and labeled with their $\delta^{18}\text{O}$ value, normalized to the average value for entire grain. The spot-to-spot standard deviation for the concurrently analyzed San Carlos olivine standard was $\pm 0.42\%$, 1σ , whereas that for adjacent glass (which was presumably homogeneous in $\delta^{18}\text{O}$) was $\pm 0.35\%$, 1σ (experiment MPDA-26; $n = 10$) and $\pm 0.49\%$, 1σ (experiment MPDA-32; $n = 5$). Olivines in both experiments exhibit oxygen isotope variations ($\pm 0.25\%$, 1σ , $n = 6$, for MPDA-26; $\pm 0.39\%$, 1σ , $n = 4$, for MPDA-32) that are consistent with isotopic homogeneity within the limits of precision of our analyses.

isotope data were measured by pseudo-multicollection on the Cameca ims-7f geo and have spot-to-spot errors of ~ 0.3 to 0.4% , 1σ , rather than the $\sim 0.2\%$ errors typical of the data generated using the CAMECA ims-1280 (see the Electronic Appendix for further details). We also measured the oxygen isotope ratio of glass adjacent to these grains to provide an additional test of the external errors of our methods. However, these data cannot be used to test meaningfully for olivine–melt equilibrium because matrix effects in glass were not evaluated owing to a lack of matrix-matched glass standards.

Olivine in experiment MPDA-26 grew during relatively rapid cooling (30°C h^{-1}), resulting in skeletal growth, trapping of melt embayments in the growing crystals, and strong, variable P enrichment. These textures and P enrichment patterns bear some resemblance to the P zonation patterns in grain R215-7.2 grain 2 (Fig. 6; although we cannot quantitatively compare P variations in the X-ray maps of these synthetic grains with those in natural olivines, they appear to be of the same order of magnitude based on contrasts in count rate). Olivine in experiment MPDA-32 grew during slower cooling (1°C h^{-1}), resulting in more equant, inclusion-free grains that exhibit oscillatory zonation in P (resembling P zonation patterns seen in natural grains that are homogeneous in $\delta^{18}\text{O}$; Fig. 5). Olivine in both synthetic samples is homogeneous in $\delta^{18}\text{O}$, within our ability to resolve: olivine in MPDA-26 varies in $\delta^{18}\text{O}$ by $\pm 0.25\%$, 1σ (spot-to-spot) and that in MPDA-32 by $\pm 0.39\%$, whereas olivine standards and glasses (which are probably homogeneous in $\delta^{18}\text{O}$ at this length scale) analyzed concurrently with these samples each varied internally by ± 0.35 to ± 0.42 (1σ , spot-to-spot). Our analyses of olivines in samples MPDA-26 and -32 included both relatively P-rich and P-poor domains from the same grains; thus, if the processes of non-equilibrium growth responsible for P enrichment in rapidly growing olivine inevitably led to per-mil level oxygen isotope variations, we should have seen a larger range in $\delta^{18}\text{O}$ (and, if the pattern resembled that in grain R215-7.2 grain 2, lower $\delta^{18}\text{O}$ in the more P-rich domains).

Our analytical results for these experiments demonstrate that olivine phenocrysts grown in a closed system can develop zonation and non-equilibrium enrichments in P with no detectable variations in $\delta^{18}\text{O}$. It should be noted that this is not a clear demonstration that these synthetic olivines grew in oxygen isotopic equilibrium with their host melts (i.e. because we could not measure the coexisting glass with the requisite accuracy by SIMS). Thus, this result is consistent with but does not require that oxygen isotopes maintain or closely approach local exchange equilibrium between melts and growing crystals despite large departures from equilibrium with respect to partitioning of at least some trace elements (Milman-Barris *et al.*, 2008). However, this result clearly differs from the $\delta^{18}\text{O}$ –P

systematics of sample R215-7.2 grain 2 (Figs 6 and 7) and thus does not support the hypothesis that oxygen isotope variations in that sample result from non-equilibrium growth.

DISCUSSION

The results of this study indicate that oxygen isotopes in both natural and synthetic olivines are typically homogeneous at our current detection limits, even in grains that exhibit pronounced oscillatory and skeletal zonation in P and from environments known to have magmas with considerable oxygen isotope variability (e.g. Iceland). This suggests that non-equilibrium processes such as diffusion-limited growth or surface entrapment—which are hypothesized to cause enrichments of P and other incompatible trace elements in igneous minerals—and/or the processes leading to variability in oxygen isotopes between magmas from a single environment do not typically lead to significant oxygen isotope variations during the growth of single phenocrysts in mafic rocks. If this result is general, it follows that the exception to this generalization, Mauna Kea sample R215-7.2 grain 2, reflects some idiosyncratic process particular to that sample.

One possibility, consistent with prior study of the oxygen isotope geochemistry of Hawaiian lavas (Eiler *et al.*, 1996; Garcia *et al.*, 1998, 2008; Wang & Eiler, 2008), is that oxygen isotope zonation in this grain records variations in composition (spatially and/or temporally) of its parent magma caused by variable mixing between a primitive basaltic melt having $\delta^{18}\text{O}$ similar to most terrestrial basalts ($\delta^{18}\text{O}_{\text{SMOW}}$ of olivine $\sim 5.2 \pm 0.2\%$) and a low- $\delta^{18}\text{O}$ contaminant (at least as low as melt in equilibrium with the lowest $\delta^{18}\text{O}$ olivine observed in this study; i.e. $\sim 3.5\%$) derived from hydrothermally altered rocks in the volcanic edifice. In the context of this hypothesis, exceptionally low- $\delta^{18}\text{O}$ portions of the grain would be interpreted as the products of nucleation immediately after contamination, perhaps with strong undercooling associated with the mixing process leading to rapid crystal growth and ‘feathery’, P-rich, skeletal olivine growth. Most of the olivine then grew from a relatively homogeneous mixture richer in primitive melt, and thus higher in $\delta^{18}\text{O}$. Finally, the highest $\delta^{18}\text{O}$ values seen in this grain (up to 5.4%) may have grown from melt having a $\delta^{18}\text{O}$ consistent with primitive, mantle-derived melt; a similar result was previously obtained from *in situ* laser fluorination measurements of large Mauna Kea phenocrysts (Wang & Eiler, 2008), and a broadly similar interpretation was suggested by a previous ion probe study of oxygen isotope variations in Icelandic olivines by Bindeman *et al.* (2008b). This progression would be consistent with the isotopic evolution of a magma chamber that is contaminated by wall-rock and then purged by primitive melt. That is, addition of a low- $\delta^{18}\text{O}$ contaminant to a primitive melt may create

short-lived heterogeneities in $\delta^{18}\text{O}$, temperature and perhaps other properties (such as nucleation sites from partially dissolved contaminant solids or mixing of magmas), and phenocrysts could preferentially nucleate in the coldest, lowest- $\delta^{18}\text{O}$, most contaminant-rich domains or as a result of the generation of undercooling during the mixing process (e.g. Walker *et al.*, 1979). However, mixing will eventually diminish these heterogeneities, so subsequent olivine growth on early formed, low- $\delta^{18}\text{O}$, P-rich cores will be slower and draw on a more homogeneous and, on average, less contaminated parent melt. Although other explanations of our observations are probably possible, this scenario is consistent with recent work on the sources of low- $\delta^{18}\text{O}$ materials in Kilauea's east rift zone and the mechanisms by which those materials are mixed into relatively primitive melts (Garcia *et al.*, 2008). It should be noted, however, that it is also possible that the coupled P enrichment and ^{18}O depletion recorded in the anomalous Mauna Kea grain reflects addition of a P-rich, low- $\delta^{18}\text{O}$ component to the melt during the contamination event rather than non-equilibrium P partitioning during rapid olivine growth. The high amplitude of P variations in this grain would require exceptionally high P contents in the melt, at least locally, but this might be possible if the low- $\delta^{18}\text{O}$ contaminant is a partial melt of hydrothermally altered rock that is enriched in incompatible elements relative to the basalts and/or gabbros from which it is derived.

SUMMARY AND CONCLUSIONS

- (1) Our findings suggest that oxygen isotope heterogeneity at a level detectable by current ion microprobe techniques (*c.* $\pm 0.2\%$, 1σ , spot-to-spot reproducibility) is unusual, and that pronounced heterogeneity—a large multiple of analytical precision—is rare (observed in only one out of 34 grains in this study). If this result is representative, it suggests that oxygen isotope compositions (unlike Fe and Li isotopes) in mafic and ultramafic terrestrial rocks are generally homogeneous and thus usually well represented by conventional analyses of mineral separates.
- (2) At least some of the natural grains we find to be homogeneous in $\delta^{18}\text{O}$ exhibit oscillatory and more complex zonation in P. Thus, although the enrichment and variability in P in the olivine is probably due to non-equilibrium processes such as diffusion-limited growth and/or surface entrapment, these non-equilibrium processes do not appear to significantly influence oxygen isotope partitioning into growing olivine. This result is consistent with our analysis of synthetic olivines that have non-equilibrium P zonation but are homogeneous in oxygen isotope ratios.
- (3) We discovered large ($>1\%$) oxygen isotope variations within one Hawaiian olivine grain (R215-7.2 grain 2 from a subaerial Mauna Kea tholeiite) and showed that these variations are associated with enrichments in P. Although this result could be consistent with coupled non-equilibrium partitioning of P and oxygen isotopes between melt and olivine in this case, the fact that these elements are decoupled in other natural samples and in the synthetic olivines suggests otherwise. We hypothesize that the pattern of zonation seen in this single olivine is a record of rapid olivine growth in response to contamination by low- $\delta^{18}\text{O}$, hydrothermally altered materials from the volcanic edifice.
- (4) The data presented here demonstrate that a large-radius multi-collector ion microprobe can generate data with precision and (after correction to an appropriate standard) accuracy sufficient to study the subtle ($\sim 1\%$) oxygen isotope variations characteristic of silicate minerals in mafic and ultramafic rocks. Our data for Icelandic sample 98MI demonstrate the potential of this approach for studying intercrystalline oxygen isotope variations within single hand samples or thin sections, and our data for Hawaiian basalt R215-7.2 show its utility for the study of intracrystalline zonation. However, this demonstration of the potential of this technique comes with a caveat: subtle oxygen isotope variations can be studied reliably only when samples are prepared according to the recommendations of Valley & Kita (2009) and analytical methods maximize spot size and beam current. Compromise on either count degrades spot-to-spot reproducibility by at least a factor of two, thereby preventing meaningful study of approximately per mil amplitude oxygen isotope variations. It is unclear whether these approaches can be extended with similar success and with similar detection limits to *in situ* studies of isotopic variations in other stable isotope systems (e.g. Fe, Mg or Si); this is an attractive target for future studies, and could be helpful in interpreting recent findings of isotopic variations in these elements at scales of single grains (Teng *et al.*, 2008).
- (5) There are two limitations of the work presented here. First, our survey of a few dozen grains from five rocks is the broadest exploration to date of intracrystalline oxygen isotope zonation of minerals in mafic and ultramafic rocks. Nevertheless, it is not exhaustive and therefore there is some risk that it is not representative. It seems likely to us, based on our results for sample R215-7.2 and previous studies of Icelandic lavas (e.g. Bindeman *et al.*, 2008*b*), that intracrystalline oxygen isotope zonation may be common in environments in which magmas assimilate low- $\delta^{18}\text{O}$ hydrothermally altered rocks. Second, future work

should use similar methods to examine rock types not considered here, such as komatiites, mantle eclogites and pyroxenites, and arc basalts. Furthermore, although the particular synthetic materials we examined appear to be homogeneous in oxygen isotope ratio (within the limits of precision of our methods), perhaps one could experimentally grow olivines that are zoned in oxygen isotope ratio through precipitation from a silicate melt, provided that growth rates or supercoolings were sufficient. Even if one could only do so by exploring melt compositions and/or cooling rates outside the range of natural environments, such experiments could place bounds on the physical conditions implied by the homogeneous grains that appear to be the rule.

ACKNOWLEDGEMENTS

We thank Yunbin Guan and Ma Chi for assistance in the Caltech ion microprobe and electron microprobe laboratories, and the staff of the WiscSIMS laboratory for assistance with sample preparation, characterization and analysis. Noriko Kita, Takayuki Ushikubo, and John Valley assisted with analyses at WiscSIMS. We thank Mike Baker for his assistance with electron microprobe analyses of several of the samples examined in this study. This study benefited from thorough, helpful reviews by Colin Macpherson, Ilya Bindeman and one anonymous reviewer, and from the editorial comments of Marjorie Wilson.

FUNDING

This work was supported by funding from the NSF-EAR program to J.M.E. and E.M.S., by partial funding of the WiscSIMS laboratory by the NSF-EAR program (0319230, 0516725, 0744079), and by financial support of the Moore Foundation to the Caltech Microanalysis Center.

SUPPLEMENTARY DATA

Supplementary data for this paper are available at *Journal of Petrology* online.

REFERENCES

- Baker, J. A., MacPherson, C. G., Menzies, M. A., Thirlwall, M. F., Al-Kadasi, M. & Matthey, D. P. (2000). Resolving crustal and mantle contributions to continental flood volcanism, Yemen; constraints from mineral oxygen isotope data. *Journal of Petrology* **41**, 1805–1820.
- Bindeman, I. N., Fu, B., Kita, N. T. & Valley, J. W. (2008a). Origin and evolution of silicic magmatism at Yellowstone based on ion microprobe analysis of isotopically zoned zircons. *Journal of Petrology* **49**, 163–193.
- Bindeman, I., Gurenko, A., Sigmarsson, O. & Chaussidon, M. (2008b). Oxygen isotope heterogeneity and disequilibria of olivine crystals in large volume Holocene basalts from Iceland: Evidence for magmatic digestion and erosion of Pleistocene hyaloclastites. *Geochimica et Cosmochimica Acta* **72**, 4397–4420.
- Davidson, J. P., Desilva, S. L., Holden, P. & Halliday, A. N. (1990). Small-scale disequilibrium in a magmatic inclusion and its more silicic host. *Journal of Geophysical Research* **95**, 17661.
- Davidson, J. P., Morgan, D. J., Charlier, B. L. A., Harlou, R. & Hora, J. M. (2007). Microsampling and isotopic analysis of igneous rocks: Implications for the study of magmatic systems. *Annual Review of Earth and Planetary Sciences* **35**, 273–311.
- Eiler, J. M. (2001). Oxygen isotope variations of basaltic lavas and upper mantle rocks. In: Valley, J. W. & Cole, D. R. (eds) *Stable Isotope Geochemistry. Mineralogical Society of America and Geochemical Society, Reviews in Mineralogy and Geochemistry* **43**, 319–364.
- Eiler, J. M., Farley, K., Valley, J. W., Stolper, E. M., Hauri, E. & Craig, H. (1995). Oxygen isotope evidence against bulk recycled sediment in the source of Pitcairn Island lavas. *Nature* **377**, 138–141.
- Eiler, J. M., Farley, K. A., Valley, J. W., Hofmann, A. & Stolper, E. M. (1996). Oxygen isotope constraints on the sources of Hawaiian volcanism. *Earth and Planetary Science Letters* **144**, 453–468.
- Eiler, J. M., Graham, C. & Valley, J. W. (1997). SIMS analysis of oxygen isotopes: Matrix effects in complex minerals and glasses. *Chemical Geology* **138**, 221–244.
- Eiler, J. M., Gronvold, K. & Kitchen, N. (2001). Oxygen isotope evidence for the origin of chemical variations in lavas from Theistareykir volcano in Iceland's northern volcanic zone. *Earth and Planetary Science Letters* **184**, 269–286.
- Eiler, J. M., Carr, M. J., Reagan, M. & Stolper, E. (2005). Oxygen isotope constraints on the sources of Central American arc lavas. *Geochemistry, Geophysics, Geosystems* **6**, article number Q07007, doi: 10.1029/2004GC000804.
- Eiler, J. M., Schiano, P., Valley, J. W., Kita, N. T. & Stolper, E. M. (2007). Oxygen-isotope and trace element constraints on the origins of silica-rich melts in the subarc mantle. *Geochemistry, Geophysics, Geosystems* **8**, article number Q09012, doi: 10.1029/2006GC001503.
- Fourcade, S., Maury, R. C., Defant, M. J. & McDermott, F. (1994). Mantle metasomatic enrichment versus arc crust contamination in the Philippines—oxygen isotope study of Batan ultramafic nodules and northern Luzon arc lavas. *Chemical Geology* **114**, 199–215.
- Gallagher, K. & Elliott, T. (2009). Fractionation of lithium isotopes in magmatic systems as a natural consequence of cooling. *Earth and Planetary Science Letters* **278**, 286–296.
- Garcia, M. O., Ito, E., Eiler, J. M. & Pietruszka, A. J. (1998). Crustal contamination of Kilauea Volcano magmas revealed by oxygen isotope analyses of glass and olivine from Puu Oo eruption lavas. *Journal of Petrology* **39**, 803–817.
- Garcia, M. O., Ito, E. & Eiler, J. M. (2008). Oxygen isotope evidence for chemical interaction of Kilauea historical magmas with basement rocks. *Journal of Petrology* **49**, 757–769.
- Griffin, W. L., Smith, D., Ryan, C. G., O'Reilly, S. Y. & Win, T. T. (1996). Trace-element zoning in mantle minerals: Metasomatism and thermal events in the upper mantle. *Canadian Mineralogist* **34**, 1179–1193.
- Griffin, W. L., Wang, X., Jackson, S. E., Pearson, N. J., O'Reilly, S. Y., Xu, X. S. & Zhou, X. M. (2002). Zircon chemistry and magma mixing, SE China: *in situ* analysis of Hf isotopes, Tonglu and Pingtan igneous complexes. *Lithos* **61**, 237–269.
- Grimes, C. B., Ushikubo, T., John, B. E. & Valley, J. W. (2011). Uniformly mantle-like $\delta^{18}\text{O}$ in zircons from oceanic plagiogranites and gabbros. *Contributions to Mineralogy and Petrology* **161**, 13–33.
- Hanchar, J. M. & Miller, C. F. (1993). Zircon zonation patterns as revealed by cathodoluminescence and backscattered electron

- images—implications for interpretation of complex crustal histories. *Chemical Geology* **110**, 1–13.
- Hattori, K. & Sato, H. (1996). Magma evolution recorded in plagioclase zoning in 1991 Pinatubo eruption products. *American Mineralogist* **81**, 982–994.
- Hawkesworth, C. J., Blake, S., Evans, P., Hughes, R., MacDonald, R., Thomas, L. E. & Turner, S. P. (2000). Time scales of crystal fractionation in magma chambers—integrating physical, isotopic and geochemical perspectives. *Journal of Petrology* **41**, 991–1006.
- Hofmann, A. E., Valley, J. W., Watson, E. B., Cavosie, A. J. & Eiler, J. M. (2009). Sub-micron scale distributions of trace elements in zircon. *Contributions to Mineralogy and Petrology* **158**(3), 317–335.
- Jambon, A. (1980). Isotopic fractionation—a kinetic-model for crystals growing from magmatic melts. *Geochimica et Cosmochimica Acta* **44**, 1373–1380.
- Jeffcoate, A. B., Elliott, T., Kasemann, S. A., Ionov, D., Cooper, K. & Brooker, R. (2007). Li isotope fractionation in peridotites and mafic melts. *Geochimica et Cosmochimica Acta* **71**, 202–218.
- Jeffries, T. E., Perkins, W. T. & Pearce, N. I. G. (1995). Measurements of trace-elements in basalts and their phenocrysts by laser probe microanalysis inductively-coupled plasma-mass spectrometry (LPMA-ICP-MS). *Chemical Geology* **121**, 131–144.
- Kita, N. T., Ushikubo, T., Fu, B. & Valley, J. W. (2009). High precision SIMS oxygen isotope analysis and the effect of sample topography. *Chemical Geology* **264**, 43–57.
- Kuritani, T. (1998). Boundary layer crystallization in a basaltic magma chamber: evidence from Rishiri Volcano, Northern Japan. *Journal of Petrology* **39**, 1619–1640.
- Mattey, D., Lowry, D. & Macpherson, C. (1994). Oxygen-isotope composition of mantle peridotite. *Earth and Planetary Science Letters* **128**, 231–241.
- Maury, R. C., Defant, M. J. & Joron, J. L. (1992). Metasomatism of the sub-arc mantle inferred from trace elements in Philippine xenoliths. *Nature* **360**, 661–663.
- McCanta, M. C., Beckett, J. R., Baker, M. B. & Stolper, E. M. (2009). Minor element substitution in olivine: An experimental study. *EOS Transactions, American Geophysical Union* **90**(52), Fall Meeting Supplement, Abstract V44A-07.
- Milman-Barris, M., Beckett, J. R., Baker, M. B., Hofmann, A. E., Morgan, Z., Crowley, M., Vielzeuf, D. & Stolper, E. M. (2008). Zoning of phosphorus in magmatic olivine. *Contributions to Mineralogy and Petrology* **155**, 739–765.
- Page, F. Z., Kita, N. T. & Valley, J. W. (2010). Ion microprobe analysis of oxygen isotopes in garnets of complex chemistry. *Chemical Geology* **270**, 9–19.
- Reddy, K. P. R., Oh, S. M., Major, L. D. & Cooper, A. R. (1980). Oxygen diffusion in forsterite. *Journal of Geophysical Research* **85**, 322–326.
- Richard, M., Maury, R., Bellon, H., Stephan, J. F., Boirat, J. M. & Calderon, A. (1986). Geology of Mt. Iraya volcano and Batan island, northern Philippines. *Philipp. J. Volcanol.* **3**, 1–27.
- Richter, F. M., Davis, A. M., DePaolo, D. J. & Watson, E. B. (2003). Isotope fractionation by chemical diffusion between molten basalt and rhyolite. *Geochimica et Cosmochimica Acta* **67**, 3905–3923.
- Rumble, D., Farquhar, J., Young, E. D. & Christensen, C. P. (1997). *In situ* oxygen isotope analysis with an excimer laser using F₂ and BrF₃ reagents and O₂ gas as analyte. *Geochimica et Cosmochimica Acta* **61**, 4229–4234.
- Schiano, P., Clocchiatti, R., Shimizu, N., Maury, R. C., Jochum, K. P. & Hofmann, A. W. (1995). Hydrous, silica-rich melts in the sub-arc mantle and their relationship with erupted arc lavas. *Nature* **377**, 595–600.
- Teng, F. Z., Dauphas, N. & Helz, R. T. (2008). Iron isotope fractionation during magmatic differentiation in Kilauea Iki Lava Lake. *Science* **320**, 1620–1622.
- Valley, J. W. (2010). Magmatic zircons: evolution of δ¹⁸O through time—revisited *in situ*, Abstract presented at the 2010 Goldschmidt Conference, Knoxville, TN. *Geochimica et Cosmochimica Acta*, Suppl. 74, A1069.
- Valley, J. W. & Kita, N. (2009). In Situ Oxygen Isotope Geochemistry by Ion Microprobe. In: Fayek, M. (ed.) *Secondary Ion Mass Spectrometry in the Earth Sciences: Gleaning the Big Picture from a Small Spot*, Mineralogical Association of Canada Short Course **41**, 19–63.
- Walker, D., Shibata, T. & Delong, S. E. (1979). Abyssal tholeiites from the Oceanographer Fracture Zone. 2. Phase equilibria and mixing. *Contributions to Mineralogy and Petrology* **70**, 111–125.
- Wang, Z. (2005). Oxygen isotope studies of the petrogenesis of Hawaiian lavas and a theoretical study on equilibrium thermodynamics of multiply-substituted isotopologues, PhD thesis, California Institute of Technology, Pasadena.
- Wang, Z. R. & Eiler, J. M. (2008). Insights into the origin of low-δ¹⁸O basaltic magmas in Hawaii revealed from *in situ* measurements of oxygen isotope compositions of olivines. *Earth and Planetary Science Letters* **269**, 376–386.
- Wang, Z., Kitchen, N. E. & Eiler, J. M. (2003). Oxygen isotope geochemistry of the second HSDP core. *Geochemistry, Geophysics, Geosystems* **4**, art. no. 8712, doi: 10.1029/2002GC000406.
- Watson, E. B. (1996). Surface enrichment and trace-element uptake during crystal growth. *Geochimica et Cosmochimica Acta* **60**, 5013–5020.
- Watson, E. B. & Muller, T. (2009). Non-equilibrium isotopic and elemental fractionation during diffusion-controlled crystal growth under static and dynamic conditions. *Chemical Geology* **267**, 111–124.
- Yogodzinski, G. M. & Kelemen, P. B. (1998). Slab melting in the Aleutians: implications of an ion probe study of clinopyroxene in primitive adakite and basalt. *Earth and Planetary Science Letters* **158**, 53–65.
- Zhou, M. F., Yan, D. P., Kennedy, A. K., Li, Y. Q. & Ding, J. (2002). SHRIMP U–Pb zircon geochronological and geochemical evidence for Neoproterozoic arc-magmatism along the western margin of the Yangtze Block, South China. *Earth and Planetary Science Letters* **196**, 51–67.